Chapter 5
Automatic Control of Rockets

5.1 Aims and Objectives

- To model a rocket's attitude plant with gimbaled nozzle and reaction jet actuators
- To design and analyze a rocket's roll, pitch, and yaw control systems using single-variable and multi-variable methods

5.2 Introduction

It is crucial for a rocket to be always aligned with the velocity vector due to aerodynamic load considerations. It is easy to appreciate the fragility of the thin structure of a rocket filled with liquid propellants – much like an elongated aluminum can of soda – for which any significant transverse acceleration due to lift (or sideforce) can prove to be destructive. The solid propellant rockets are structurally more robust, but suffer from another fallibility common to all rockets: inherent aerodynamic instability with respect to angle-of-attack, α, (or sideslip, β). A small error in either α or β – if uncorrected – can quickly build-up, leading to excessive transverse loads that are certain to destroy the vehicle. For this reason, all rockets are axisymmetric in shape and mass distribution, which enables an equilibrium flight condition without a net lift and sideforce. In order to correct attitude deviations from equilibrium, most rockets are also equipped with an attitude control system for making the vehicle follow the desired flight path, such that angle-of-attack and sideslip angle are always zero. Such a control system applies its control forces and moments through aerodynamic control surfaces and thrust deflection. Rocket maneuvers are performed by generating a pure torque (without a net lateral force), which causes the large rocket thrust to act in a new direction. Smaller rockets – such as air-to-air missiles – have movable fins mounted fore and aft of the center of mass in a way similar to aircraft lifting surfaces. However, the fins are much smaller than the wings and tails of an aircraft, because they are intended

A. Tewari, *Automatic Control of Atmospheric and Space Flight Vehicles: Design and Analysis with MATLAB® and Simulink®*, Control Engineering,
DOI 10.1007/978-0-8176-4864-0_5,

for stability and control rather than for lift generation. For achieving longitudinal (pitch-yaw) stability at lower altitudes, large rockets – such as launch vehicles and ballistic missiles – are also fitted with small aerodynamic fins near the base. If made movable, the fins can apply small control torques in the denser region of the atmosphere (such as in the case of German *V-2* rocket of WW-II). However, since a launch vehicle operates at a wide range of speeds and altitudes, one cannot rely upon the small aerodynamic moments generated by movable fins to control the vehicle throughout its trajectory. Instead, the primary control torque is generated by a combination of thrust-vectoring, i.e., by changing the direction of the thrust vector relative to the axis of symmetry, and through cold gas reaction jets firing normal to the axis. Some vehicles also have separate (but small) vernier rockets for making fine adjustments in overall thrust magnitude and direction.

All rockets are statically unstable in pitch and yaw ($M_\alpha > 0, N_\beta < 0$). They are also unstable in roll when not stabilized by large aerodynamic fins. Hence, rockets require active stabilization via a fully gimbaled, gyro-stabilized platform called an *inertial measurement unit* (IMU) (Chap. 2) consisting of pendulum switches, rate gyros, and accelerometers. The IMU can sense multi-axis angle and angular rate deviations and thus lies at the heart of the rocket's control system. Digital electronics have enabled the replacement of the fully gimbaled platforms by *strap-on IMU* units rigidly attached to the vehicle for better resolution, ruggedness, and smaller weight. These units have fewer moving parts, and mainly rely upon solid-state accelerometers, tuning forks, quartz oscillators, and ring laser gyros. The guidance system continuously sends attitude commands to be tracked by the controller. With the available commands and actual sensor data, the attitude controller drives the nozzle gimbals and/or reaction gas jets to nullify the attitude errors. Apart from sending the nominal attitude, the guidance system also performs minor trajectory corrections by directly driving the gimbal actuators.

5.2.1 Thrust Vectoring for Attitude Control

Creation of attitude control torque by thrust vectoring requires a balancing of the transverse forces. Thus, a minimum number of two equal and opposite control forces is necessary to form a pure couple. While a short-range missile operating entirely inside the lower atmosphere can have the control force produced by an aerodynamic fin to oppose that produced by vectored thrust, this is not feasible for a gravity-turn launch vehicle. In a launch vehicle, thrust-vectoring can be mainly achieved in three distinct ways:[1] (a) gimbaling of a single main engine balanced by reaction jets or vernier rockets, (b) gimbaling of two or more main engines, and (c) differential

[1]Some short-range rockets – such as the German *V-2* and the Russian *SCUD* – alternatively use graphite vanes at nozzle exit to generate limited control moments by rotation and deflection of the exhaust gases.

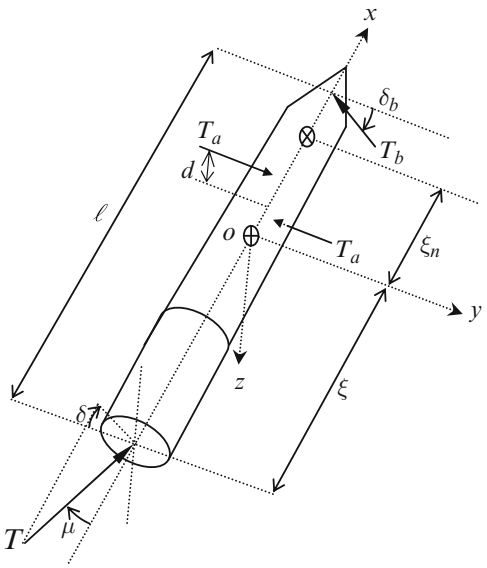

Fig. 5.1 Thrust-vectoring geometry for a rocket equipped with a single gimbaled engine, a balancing reaction jet, and a pair of roll reaction jets

thrust from gimbaled nozzles. Some launch vehicles (such as the erstwhile "Space Shuttle" of NASA) use (a) and (b) alternatively in different stages. The concept of differential thrust for attitude control has not been used due to practical limitations.

5.2.1.1 Reaction Jet System

Gimbaling a single rocket engine can produce pitching and yawing control moments about the center of mass. However, for static stability, one must also have a set of smaller vernier rockets (or gas jets) mounted on the other side of the center of mass that are capable of balancing the sideforce generated by the gimbaled nozzle, by creating a small thrust of their own. In the absence of a balancing thrust, the vehicle has a tendency to move sideways in a destructive manner, if not controlled by a closed-loop system. Consider a rocket with principal body-fixed frame, $oxyz$. Thrust vectoring consists of a gimbaled rocket nozzle at the base that swivels in any desired direction, δ, measured from oz, and deflects by a small thrust angle, μ, measured from ox as shown in Fig. 5.1. The distance of gimbaled nozzle is ξ from the center of mass o and ℓ from the balancing jet. The reaction jets/vernier rockets can be mounted in a ring-like fashion to provide transverse force balance for a particular swivel angle, δ. Assuming a small thrust angle, μ, and a balancing thrust, T_b, normal to the axis ox in the direction δ_b (Fig. 5.1), we have the following pitch-yaw control torque about o:

$$\boldsymbol{\tau} \simeq [T\mu\xi \sin\delta + T_b(\ell - \xi)\sin\delta_b]\,\mathbf{j} - [T\mu\xi\cos\delta + T_b(\ell - \xi)\cos\delta_b]\,\mathbf{k}. \quad (5.1)$$

Force balance requires

$$T\mu\,(\mathbf{j}\cos\delta + \mathbf{k}\sin\delta) = T_b\,(\mathbf{j}\cos\delta_b + \mathbf{k}\sin\delta_b)\,. \tag{5.2}$$

When force balance is not carried out, we have $T_b = 0$, thereby producing a net transverse force

$$\mathbf{F} \simeq T\mu\,(\mathbf{j}\cos\delta + \sin\delta\mathbf{k})\,, \tag{5.3}$$

and the pitch-yaw torque becomes

$$\boldsymbol{\tau} = T\mu\xi\,(\mathbf{j}\sin\delta - \mathbf{k}\cos\delta)\,. \tag{5.4}$$

For simplicity of notation, we define *effective deflection angles*,

$$\begin{aligned}\mu_1 &= \mu\sin\delta\\ \mu_2 &= \mu\cos\delta,\end{aligned} \tag{5.5}$$

which make the transverse force and pitch-yaw control torque the following linear functions for given values of (T, ξ):

$$\begin{aligned}\mathbf{F} &= T\,(\mu_2\mathbf{j} + \mu_1\mathbf{k})\\ \boldsymbol{\tau} &= T\xi\,(\mu_1\mathbf{j} - \mu_2\mathbf{k})\,.\end{aligned} \tag{5.6}$$

In the absence of force balance, the angles μ, δ, must be continuously manipulated by an active control system to maintain a nominal attitude. Instead, for achieving transverse control force balance, we must have

$$T\mu\cos\delta = T_b\cos\delta_b, \tag{5.7}$$

and

$$T\mu\sin\delta = T_b\sin\delta_b, \tag{5.8}$$

which implies

$$\delta = \delta_b. \tag{5.9}$$

Thus, when the transverse force balance is carried out, the control torque is given by

$$\boldsymbol{\tau} = T\mu\ell\,(\mathbf{j}\sin\delta - \mathbf{k}\cos\delta)\,, \tag{5.10}$$

or

$$\boldsymbol{\tau} = T\ell\,(\mu_1\mathbf{j} - \mu_2\mathbf{k})\,. \tag{5.11}$$

Clearly, for a given thrust angle, μ, the ratio of pitching and yawing moments can be adjusted by varying the swivel angle, δ. For a nominal gravity-turn trajectory, we select oxz as the vertical plane. Hence, $\delta = \pi/2$ and we have a pure pitching moment. Note that the control torque with force balance is independent of the location of center of mass, o, that varies as the propellant is consumed. In such a case, the attitude control-law need not adapt with respect to center of mass variation.

In order to correct small, off-nominal deviations from the vertical plane, there must be an additional capability to generate a small rolling control moment by a pair of roll reaction jets or vernier rockets of thrust, T_a, applied at an offset, d, from ox (Fig. 5.1). The net control torque is thus given by

$$\boldsymbol{\tau} = 2T_a d\,\mathbf{i} + T\xi\,(\mu_1\mathbf{j} - \mu_2\mathbf{k})\,, \tag{5.12}$$

with the understanding that ξ should be replaced by ℓ in case of transverse force balance. Due to the fact that $T_a \ll T$, $d \ll \xi$, the rolling control moment is generally an order of magnitude smaller than the pitching and yawing moments. Thus, a launch vehicle equipped with reaction jet control system cannot tolerate significant off-nominal roll deviations.

5.2.1.2 Multiple Gimbaled Nozzle System

Two (or more) rocket engines can be simultaneously gimbaled by different angles to create a control torque without an unbalanced sideforce. In addition, by having a large difference in the gimbal angles, a significant rolling moment can be generated which is not feasible in a reaction jet system. Consider a rocket with a pair of gimbaled rocket nozzles of thrust T_a and T_b, respectively, symmetrically located about ox at the base, with a spacing $2d$ between them. The line joining the centers of the nozzles makes an angle σ with oy, as shown in Fig. 5.2. The nozzles can swivel in desired directions about the longitudinal axis, ox, by angles (δ_a, δ_b) and by small deflection angles (μ_a, μ_b) about the yaw axis, oz (Fig. 5.2). The net transverse force and torque produced by the two nozzles are expressed as follows:

$$\mathbf{F} \simeq (T_a\mu_a \cos\delta_a - T_b\mu_b \cos\delta_b)\mathbf{j} + (T_a\mu_a \sin\delta_a - T_b\mu_b \sin\delta_b)\mathbf{k}. \tag{5.13}$$

$$\begin{aligned}
\boldsymbol{\tau} \simeq\ & [-\xi\mathbf{i} - d(\cos\sigma\mathbf{j} + \sin\sigma\mathbf{k})] \times T_a(\mathbf{i} + \mu_a \cos\delta_a\mathbf{j} + \mu_a \sin\delta_a\mathbf{k}) \\
& + [-\xi\mathbf{i} + d(\cos\sigma\mathbf{j} + sin\sigma\mathbf{k})] \times T_b(\mathbf{i} - \mu_b \cos\delta_b\mathbf{j} - \mu_b \sin\delta_b\mathbf{k}) \\
=\ & d\,[\sin\sigma\,(T_a\mu_a \cos\delta_a + T_b\mu_b \cos\delta_b) - \cos\sigma\,(T_a\mu_a \sin\delta_a + T_b\mu_b \sin\delta_b)]\,\mathbf{i} \\
& + [d\,\sin\sigma(T_b - T_a) + \xi\,(T_a\mu_a \sin\delta_a - T_b\mu_b \sin\delta_b)]\,\mathbf{j} \\
& + [d\,\cos\sigma(T_a - T_b) + \xi\,(T_b\mu_b \cos\delta_b - T_a\mu_a \cos\delta_a)]\,\mathbf{k}.
\end{aligned}$$

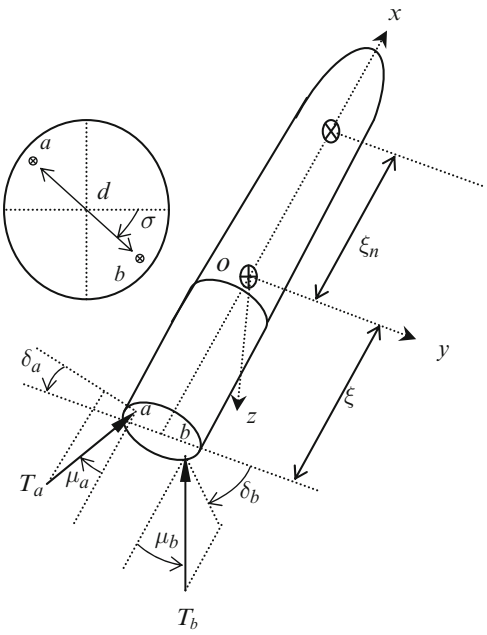

Fig. 5.2 Thrust vectoring geometry for a rocket equipped with a pair of gimbaled engines at the base

For simplifying the notation, we define *effective deflection angles* as

$$\begin{aligned}
\nu_1 &= \frac{1}{T}\left(T_a \mu_a \sin\delta_a - T_b \mu_b \sin\delta_b\right) \\
\nu_2 &= \frac{1}{T}\left(T_a \mu_a \cos\delta_a - T_b \mu_b \cos\delta_b\right) \\
\nu_3 &= \frac{1}{T}\left(T_a \mu_a \sin\delta_a + T_b \mu_b \sin\delta_b\right) \\
\nu_4 &= \frac{1}{T}\left(T_a \mu_a \cos\delta_a + T_b \mu_b \cos\delta_b\right),
\end{aligned} \tag{5.14}$$

which reduce the transverse force to the form of (5.6),

$$\mathbf{F} = T\left(\nu_2 \mathbf{j} + \nu_1 \mathbf{k}\right) \tag{5.15}$$

while the control torque is given by

$$\begin{aligned}
\boldsymbol{\tau} = {} & Td\left(\nu_4 \sin\sigma - \nu_3 \cos\sigma\right)\mathbf{i} + \left[-T\xi\nu_1 - d\,\sin\sigma\left(T_a - T_b\right)\right]\mathbf{j} \\
& + \left[-T\xi\nu_2 + d\,\cos\sigma\left(T_a - T_b\right)\right]\mathbf{k}.
\end{aligned} \tag{5.16}$$

Clearly, without force balance, the control torque is dependent on the changing location of center of mass, ξ. Most rocket engines are incapable of throttling fast

enough to rapidly achieve a thrust differential, $(T_a - T_b)$, required for attitude control. Thus, we generally have $T_a = T_b = T/2$ and the control torque is entirely produced by gimbaling. Almost all launch vehicles use multiple, gimbaled nozzles. The largest such system actually flown was the first stage of the *Saturn-V* rocket of NASA's *Apollo* program, in which four outboard engines achieved attitude control via gimbaling, but without differential thrust. Therefore, transverse force balance could not be achieved when pitch-yaw control was carried out.

5.2.1.3 Gimbaling with Differential Thrust

Suppose a futuristic rocket engine has the combined capability of gimbaling as well as rapid differential thrust of its two nozzles. Then transverse force balance dictates that $\nu_1 = \nu_2 = 0$, i.e.,

$$T_a \mu_a \cos\delta_a = T_b \mu_b \cos\delta_b, \tag{5.17}$$

and

$$T_a \mu_a \sin\delta_a = T_b \mu_b \sin\delta_b, \tag{5.18}$$

which have several possible solutions, the trivial one being

$$\begin{aligned} T_a &= T_b \\ \delta_a &= \delta_b \\ \mu_a &= \mu_b. \end{aligned} \tag{5.19}$$

In order to achieve force balance for an arbitrary control torque, the actuation of the nozzles must be carried out in unison such that (5.17) and (5.18) are satisfied. Clearly, a rigid axle connecting the nozzles, or a fixed gearing arrangement between them is ruled out. There must be a nonlinear, feedback actuator that generates the net thrust and the commanded torque by suitably adjusting the thrust magnitudes and deflection angles of the nozzles. For a total thrust, T, with transverse force balance, the respective nozzle thrusts are related by

$$T_a + T_b \simeq T, \tag{5.20}$$

and the net control torque is given by

$$\boldsymbol{\tau} = 2T_a \mu_a d\,\mathbf{i}\sin(\sigma - \delta_a) + d(T - 2T_a)\left[\mathbf{j}\sin\sigma - \mathbf{k}\cos\sigma\right]. \tag{5.21}$$

In order to conform with the conventional terminology, we can define *effective deflection angles* by

$$\begin{aligned} \mu_1 &= d\left(1 - 2\frac{T_a}{T}\right)\sin\sigma \\ \mu_2 &= d\left(1 - 2\frac{T_a}{T}\right)\cos\sigma, \end{aligned} \tag{5.22}$$

and the control rolling moment by

$$\tau_x = 2T_a \mu_a d. \tag{5.23}$$

Note that with force balance, the pitching and yawing moments are entirely generated by thrust differential, $(T_a - T_b)$, while the rolling moment is produced by the thrust deflection, μ_a. By having a differential thrust modulation, $(T_a - T_b)$, a much larger range of pitching and yawing moments can be generated compared with the reaction jet as well as gimbaled nozzle (without differential thrust) systems.

In summary, for a generic thrust-deflection model without either force balance or thrust differential, we have the following control forces and moments:

$$\begin{aligned} F_y &\simeq T\mu_2 \\ F_z &\simeq T\mu_1 \\ \tau_y &\simeq T\xi\mu_1 \\ \tau_z &\simeq -T\xi\mu_2. \end{aligned} \tag{5.24}$$

With force balance, we have

$$\begin{aligned} F_y &\simeq 0 \\ F_z &\simeq 0 \\ \tau_y &\simeq T\ell\mu_1 \\ \tau_z &\simeq -T\ell\mu_2. \end{aligned} \tag{5.25}$$

The expression for rolling moment, τ_x, depends upon whether the reaction jet or gimbaling with differential thrust is used.

5.3 Attitude Control Plant

Consider the following translational kinetics equations for a rocket, which are the same as those derived in Chap. 4 for an aircraft:

$$\begin{aligned} X - mg\sin\Theta &= m(\dot{U} + QW - RV) \\ Y + mg\sin\Phi\cos\Theta &= m(\dot{V} + RU - PW) \\ Z + mg\cos\Phi\cos\Theta &= m(\dot{W} + PV - QU), \end{aligned} \tag{5.26}$$

where the Euler angle sequence, $(\Psi)_3, (\Theta)_2, (\Phi)_1$, represents the orientation of the principal body frame, $(\mathbf{i}, \mathbf{j}, \mathbf{k})$, with respect to an inertial reference frame, $(\mathbf{I}, \mathbf{J}, \mathbf{K})$. However, we are no longer making the assumption that $(\mathbf{I}, \mathbf{J}, \mathbf{K})$ is approximated by

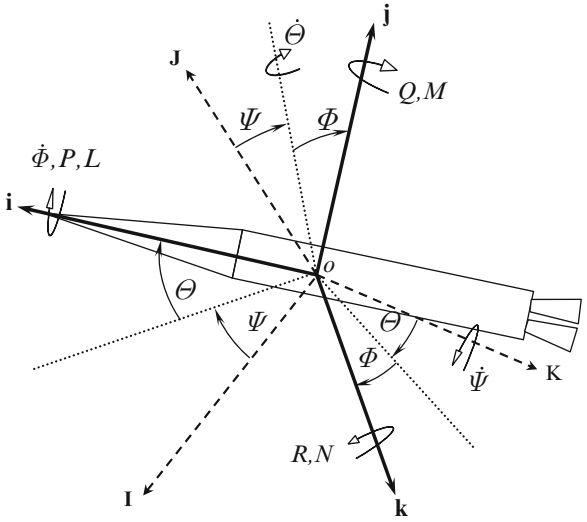

Fig. 5.3 Attitude dynamics of a rocket

the local horizon frame (which we did for the case of aircraft). The typical speed and altitude of a rocket are much higher than those of the aircraft. Consequently, the acceleration terms due to flight path curvature cannot be neglected, and the angular velocity vector,

$$\boldsymbol{\omega} = P\mathbf{i} + Q\mathbf{j} + R\mathbf{k}, \tag{5.27}$$

is measured in the inertial frame. The form of the rotational kinematics equations are unchanged from Chap. 4,

$$\begin{Bmatrix} \dot{\Phi} \\ \dot{\Theta} \\ \dot{\Psi} \end{Bmatrix} = \frac{1}{\cos\Theta} \begin{pmatrix} \cos\Theta & \sin\Phi\sin\Theta & \cos\Phi\sin\Theta \\ 0 & \cos\Phi\cos\Theta & -\sin\Phi\cos\Theta \\ 0 & \sin\Phi & \cos\Phi \end{pmatrix} \begin{Bmatrix} P \\ Q \\ R \end{Bmatrix}, \tag{5.28}$$

provided we remember that the roll angle, Φ, the pitch angle, Θ, and the yaw angle, Ψ, are now measured from the inertial (rather than local horizon) frame.

Another crucial difference between a rocket and an aircraft is that the rocket has a principal axis of symmetry, $\mathbf{i}$, which yields $J_{yy} = J_{zz}$ and $J_{xy} = J_{xz} = J_{yz} = 0$. The attitude dynamics of rockets is greatly simplified by the presence of the axis of symmetry, ox, (Fig. 5.3), resulting in the following rotational kinetics equations:

$$L = J_{xx}\dot{P}, \tag{5.29}$$

$$M = J_{yy}\dot{Q} + \left(J_{xx} - J_{yy}\right)PR, \tag{5.30}$$

$$N = J_{yy}\dot{R} + \left(J_{yy} - J_{xx}\right)PQ. \tag{5.31}$$

5.3.1 Equilibrium Conditions and Small Perturbations

It is clear from (5.26)–(5.31) that the rocket flight equations have the following equilibrium solutions (denoted by the subscript e):

(a) Steady Rolling Motion: $V_e = W_e = Q_e = R_e = 0$ and U_e, P_e constants. The resulting forces and moments at equilibrium are given by

$$\begin{aligned} X_e - mg\sin\Theta_e &= 0 \\ Y_e + mg\sin\Phi_e\cos\Theta_e &= 0 \\ Z_e + mg\cos\Phi_e\cos\Theta_e &= 0 \\ \dot{\Phi}_e &= P_e \\ \dot{\Theta}_e &= 0 \\ \dot{\Psi}_e &= 0, \end{aligned} \tag{5.32}$$

and $L_e = M_e = N_e = 0$.

(b) Steady Pitching Motion: $\Phi_e = V_e = W_e = P_e = R_e = 0$ and U_e, Q_e constants. The resulting forces and moments at equilibrium are given by

$$\begin{aligned} X_e - mg\sin\Theta_e &= 0 \\ Y_e &= 0 \\ Z_e + mg\cos\Theta_e &= -mQ_eU_e \\ \dot{\Phi}_e &= 0 \\ \dot{\Theta}_e &= Q_e \\ \dot{\Psi}_e &= 0, \end{aligned} \tag{5.33}$$

and $L_e = M_e = N_e = 0$. Since the pitch and yaw axes are indistinguishable from one another due to symmetry, here we have selected the body frame such that the constant angular velocity is given by $Q_e\mathbf{j}$. (We could have easily replaced the pitch axis with the yaw axis, and called the equilibrium solution the yawing motion. However, this is not the standard practice.)

In the linearized dynamic models given in (a) and (b) it is assumed that the aerodynamic force and moment perturbations are linearly dependent on the flow variables[2] (u, V, W, p, q, R) as well as the control inputs (μ_1, μ_2, τ_x). As for aircraft in Chap. 4, these relationships are given by the following truncated Taylor series expanded about a given equilibrium solution:

[2]Since $V = W = R = 0$ for each of the two equilibria, we will denote the perturbations in sideslip (V), downward speed (W), and yaw-rate, (R), by capital letters.

Thus, a rocket's attitude control system can be designed for maintaining the vehicle close to either of the two equilibrium points. As in the case of aircraft, the linearized equations of motion in terms of small perturbation variables, $u, v, w, \phi, \theta, \psi, p, q, R, \bar{X}, \bar{Y}, \bar{Z}$, are expressed as follows:

$$\begin{aligned}
\bar{X} &= X_u u + X_\alpha \alpha + X_{\dot{\alpha}} \dot{\alpha} + X_q q + X_{\mu_1} \mu_1 + X_{\mu_2} \mu_2 \\
\bar{Z} &= Z_u u + Z_\alpha \alpha + Z_{\dot{\alpha}} \dot{\alpha} + Z_q q + Z_{\mu_1} \mu_1 \\
\bar{M} &= M_u u + M_\alpha \alpha + M_{\dot{\alpha}} \dot{\alpha} + M_q q + M_{\mu_1} \mu_1 \\
\bar{Y} &= Y_\beta \beta + Y_{\dot{\beta}} \dot{\beta} + Y_p p + Y_r R + Y_{\mu_2} \mu_2 \\
\bar{L} &= L_\beta \beta + L_{\dot{\beta}} \dot{\beta} + L_p p + L_r R + \tau_x \\
\bar{N} &= N_\beta \beta + N_{\dot{\beta}} \dot{\beta} + N_p p + N_r R + N_{\mu_2} \mu_2,
\end{aligned} \tag{5.34}$$

where

$$\alpha \simeq \frac{W}{U_e}; \qquad \beta \simeq \frac{V}{U_e}, \tag{5.35}$$

are the changes in the angle-of-attack and sideslip angle, respectively. Due to the absence of a significant lift (or sideforce), the unsteady aerodynamic stability derivatives, $X_{\dot{\alpha}}, Z_{\dot{\alpha}}, Y_{\dot{\beta}}$, and angular rate force derivatives, X_q, Z_q, Y_p, Y_r, are negligible for a rocket. Furthermore, the small fins do not cause a significant roll-yaw cross-coupling ($N_p \simeq 0, L_r \simeq 0$), or a roll-sideslip coupling ($L_\beta \simeq 0, L_{\dot{\beta}} \simeq 0$). Also due to the pitch-yaw symmetry, we have $Z_\alpha = Y_\beta$, $M_\alpha = -N_\beta$, and $M_q = N_r$. Finally, the change in forward force caused by a small thrust deflection can be assumed to be negligible, resulting in $X_{\mu_1} \mu_1 \simeq X_{\mu_2} \mu_2 \simeq 0$.

Note that the longitudinal forces and moments depend only upon the longitudinal variables, and lateral-directional forces and moments depend only upon the lateral-directional variables. Therefore, while the motion about the roll equilibrium is essentially an inertia coupled six degree-of-freedom motion, we have a decoupling of perturbation about the pure pitching equilibrium into *longitudinal* and *lateral* dynamics:

1. Motion about Roll Equilibrium:

$$X_u u + X_\alpha \alpha - mg\theta \cos \Theta_e = m\dot{u}$$

$$Z_\alpha \beta + Y_{\mu_2} \mu_2 + mg(\phi \cos \Phi_e \cos \Theta_e - \theta \sin \Phi_e \sin \Theta_e) = m(\dot{V} + RU_e - P_e W)$$

$$Z_u u + Z_\alpha \alpha + Z_{\mu_1} \mu_1 - mg(\phi \sin \Phi_e \cos \Theta_e + \theta \sin \Theta_e \cos \Phi_e) = m(\dot{W} + VP_e - qU_e)$$

$$\dot{\phi} = p + q \sin \Phi_e \tan \Theta_e + R \cos \Phi_e \tan \Theta_e$$

$$\dot{\theta} = q \cos \Phi_e - R \sin \Phi_e$$

$$\dot{\psi} = q \sin \Phi_e \sec \Theta_e + R \cos \Phi_e \sec \Theta_e$$

$$L_p p + \tau_x = J_{xx} \dot{p}$$

$$M_u u + M_\alpha \alpha + M_{\dot{\alpha}} \dot{\alpha} + M_q q + M_{\mu_1} \mu_1 = J_{yy} \dot{q} + \left(J_{xx} - J_{yy}\right) P_\mathrm{e} R$$
$$-M_\alpha \beta - M_{\dot{\alpha}} \dot{\beta} + N_r R + N_{\mu_2} \mu_2 = J_{yy} \dot{R} + \left(J_{yy} - J_{xx}\right) P_\mathrm{e} q.$$

Clearly, we have a linear, time-varying system with $\Phi_\mathrm{e}(t)$ as a varying coefficient. Note that here we have $q = Q$.

2. Motion about Pitch Equilibrium:

(a) Longitudinal Dynamics:

$$\begin{aligned} X_u u + X_\alpha \alpha - mg\theta \cos \Theta_\mathrm{e} &= m(\dot{u} + Q_\mathrm{e} W) \\ Z_u u + Z_\alpha \alpha + Z_{\mu_1} \mu_1 - mg\theta \sin \Theta_\mathrm{e} &= m(\dot{W} - qU_\mathrm{e} - Q_\mathrm{e} u) \\ M_u u + M_\alpha \alpha + M_{\dot{\alpha}} \dot{\alpha} + M_q q + M_{\mu_1} \mu_1 &= J_{yy} \dot{q} \\ \dot{\theta} &= q. \end{aligned} \tag{5.36}$$

(b) Lateral Dynamics:

$$\begin{aligned} \dot{\phi} &= p + R \tan \Theta_\mathrm{e} \\ \dot{\psi} &= R \sec \Theta_\mathrm{e} \\ Z_\alpha \beta + Y_{\mu_2} \mu_2 + mg\phi \cos \Theta_\mathrm{e} &= m(\dot{V} + RU_\mathrm{e}) \\ L_p p + \tau_x &= J_{xx} \dot{p} \\ -M_\alpha \beta - M_{\dot{\alpha}} \dot{\beta} + M_q R + N_{\mu_2} \mu_2 &= J_{yy} \dot{R} + \left(J_{yy} - J_{xx}\right) Q_\mathrm{e} p. \end{aligned} \tag{5.37}$$

Here, the system is linear and time-varying with $\Theta_\mathrm{e}(t)$ as the varying coefficient. Also, we have $p = P$.

5.3.2 Stability About Pitch Equilibrium

The stability of the two rocket dynamics equilibria is very important. If the motion is unstable, it quickly degenerates from being a pure rolling (or pitching) motion into a wildly tumbling and translatory motion, which ultimately leads to a wayward flight or structural failure. However, the perturbed motion can be stabilized by closed-loop control such that all perturbations other than the primary rotation are suppressed. If the perturbation variables, u, V, W, q, R, are brought to zero by a feedback regulator, a constant roll rate, P_e, could be maintained at a given speed, U_e, and pitch angle, Θ_e. Similarly, by bringing u, V, W, p, R, ϕ to zero, a constant pitch rate, Q_e, can be achieved at a given speed, U_e.

As we have seen above, there is an essential difference between motion about the two equilibria: motion about roll equilibrium is inherently coupled in all the degrees-of-freedom, whereas the motion about pitch equilibrium can be decoupled

into pitch dynamics and roll-yaw dynamics. Since control of coupled degrees-of-freedom is practically very difficult, the roll equilibrium is not feasible for a rocket in atmospheric flight (although it can be easily achieved in space flight (Chap. 6)). Thus, in this chapter we are essentially confined to the discussion of motion about the pitch equilibrium.

All large rockets have a dedicated roll control system that manages to keep the roll rate virtually zero. The pitch and yaw control systems are designed to track a small, reference pitch rate ($Q = Q_d(t)$) commanded by the guidance system, while keeping the yaw rate virtually zero. In such a case, the rocket's dynamic plant is further decoupled into what is typically called the *roll*, *pitch*, and *yaw* dynamics, given by the following (where $U \simeq U_e$):

1. Roll dynamics:

$$\begin{Bmatrix} \dot{\phi} \\ \dot{p} \end{Bmatrix} = \begin{pmatrix} 0 & 1 \\ 0 & \dfrac{L_p}{J_{xx}} \end{pmatrix} + \begin{pmatrix} 0 \\ \dfrac{1}{J_{xx}} \end{pmatrix} \tau_x. \tag{5.38}$$

2. Pitch dynamics:

$$\begin{Bmatrix} \dot{u} \\ \dot{\alpha} \\ \dot{\theta} \\ \dot{q} \end{Bmatrix} = \begin{pmatrix} \dfrac{X_u}{m} & \dfrac{X_\alpha}{m} & -g\cos\Theta_e & 0 \\ \dfrac{Z_u}{mU} & \dfrac{Z_\alpha}{mU} & -\dfrac{g}{U}\sin\Theta_e & 1 \\ 0 & 0 & 0 & 1 \\ \dfrac{M_u}{J_{yy}} + \dfrac{M_{\dot{\alpha}} Z_u}{J_{yy} mU} & \dfrac{M_\alpha}{J_{yy}} + \dfrac{M_{\dot{\alpha}} Z_\alpha}{J_{yy} mU} & -\dfrac{M_{\dot{\alpha}} g \sin\Theta_e}{J_{yy} U} & \dfrac{M_q + M_{\dot{\alpha}}}{J_{yy}} \end{pmatrix} \begin{Bmatrix} u \\ \alpha \\ \theta \\ q \end{Bmatrix} + \begin{bmatrix} 0 \\ \dfrac{T}{mU} \\ 0 \\ \dfrac{T\xi}{J_{yy}}\left(1 + \dfrac{M_{\dot{\alpha}}}{mU}\right) \end{bmatrix} \mu_1. \tag{5.39}$$

3. Yaw dynamics:

$$\begin{Bmatrix} \dot{\psi} \\ \dot{\beta} \\ \dot{R} \end{Bmatrix} = \begin{pmatrix} 0 & 0 & \sec\Theta_e \\ 0 & \dfrac{Z_\alpha}{mU} & -1 \\ 0 & -\dfrac{M_\alpha}{J_{yy}} & \dfrac{M_q}{J_{yy}} \end{pmatrix} \begin{Bmatrix} \psi \\ \beta \\ R \end{Bmatrix} + \begin{bmatrix} 0 \\ \dfrac{T}{mU} \\ -\dfrac{T\xi}{J_{yy}}\left(1 + \dfrac{M_{\dot{\alpha}}}{mU}\right) \end{bmatrix} \mu_2. \tag{5.40}$$

The success of the rocket guidance and control system thus depends upon the ability of each control subsystem (roll, pitch, yaw) to regulate the roll and yaw rates, while tracking a reference pitch rate. The decoupling of roll, pitch, and yaw dynamics indicates that one can design separate roll, pitch, and yaw control loops for a rocket. It is clear from (5.39) and (5.40) that the short-period pitch (i.e., excluding airspeed variation) and yaw dynamics are nearly identical. Therefore, one can design similar feedback loops for pitch and yaw. Of the three control loops, the roll controller must have the highest bandwidth (speed) for quickly reducing the roll rate, while the pitch and yaw controllers should maintain the vehicle's attitude along the nominal trajectory.

Example 5.1. Consider the *Vanguard* rocket with the following stability and control parameters [2] at the condition of maximum dynamic pressure, $\bar{q} = 28305\ \mathrm{N/m^2}$, with airspeed, $U_\mathrm{e} = 392\ \mathrm{m/s}$, Mach number 1.4, and mass, $m = 6513.2\ \mathrm{kg}$:

$$\begin{aligned} b &= 1.1433\ \mathrm{m} \\ S &= 1.0262\ \mathrm{m^2} \\ \xi &= 8.2317\ \mathrm{m} \\ C_{l_p} &= C_{m_{\dot{\alpha}}} = C_{z_u} = C_{m_u} = 0 \\ \Theta_\mathrm{e} &= 68.5^\circ \\ C_{z_\alpha} &= -3.13\ /\mathrm{rad} \\ C_{m_\alpha} &= 11.27\ /\mathrm{rad} \\ T &= 133202.86\ \mathrm{N} \\ J_{xx} &= 5215.1\ \mathrm{kg\,m^2} \\ J_{yy} &= 156452.8\ \mathrm{kg\,m^2} \\ \frac{b}{2U_\mathrm{e}} C_{m_q} &= -0.321\ \mathrm{s}. \end{aligned} \tag{5.41}$$

Here $b/2$ is the characteristic length and S the reference area used for nondimensionalizing the stability derivatives, e.g.,

$$C_{m_\alpha} = \frac{M_\alpha}{\bar{q} S (b/2)}\ ; \qquad C_{m_q} = \frac{U_\mathrm{e} M_q}{\bar{q} S (b/2)^2}.$$

The dimensional stability derivatives are thus obtained to be the following:

$$\begin{aligned} Z_\alpha &= Y_\beta = -90916\ \mathrm{N/rad} \\ M_\alpha &= -N_\beta = 187132.5\ \mathrm{N\,m/rad} \\ M_q &= N_r = -5330.039\ \mathrm{s}. \end{aligned} \tag{5.42}$$

The rocket has pitch and yaw thrust deflection capability in powered flight such that μ_1, μ_2 can be simultaneously changed by ± 5 deg [12]. Since the vehicle is not equipped with fins and aerodynamic control surfaces, it is crucial to maintain a non-rolling attitude, $P = 0$, in the presence of disturbances, which is achieved by dedicated roll reaction jets. The rolling moment generated by the roll reaction jets is $\tau_x = \pm 625.36$ N m, whose sign can be switched as required. The roll-control system is simply a *bang-bang* switch (Chap. 1) that applies the control torque in the desired direction as soon as roll angle error crosses $\pm 3°$ [12]. Neglecting the airspeed variations (which are typically much slower in time scale, and smaller in magnitude) caused by attitudinal motion, we have the following roll, pitch and yaw dynamics:

1. Roll dynamics:

$$\begin{Bmatrix} \dot{\phi} \\ \dot{p} \end{Bmatrix} = \begin{pmatrix} 0 & 1 \\ 0 & 0 \end{pmatrix} + \begin{pmatrix} 0 \\ 0.1199 \end{pmatrix} \text{sgn}(u_1). \tag{5.43}$$

2. Pitch dynamics:

$$\begin{Bmatrix} \dot{\alpha} \\ \dot{\theta} \\ \dot{q} \end{Bmatrix} = \begin{pmatrix} -0.0356 & -0.0233 & 1 \\ 0 & 0 & 1 \\ 1.1961 & 0 & -0.0341 \end{pmatrix} \begin{Bmatrix} \alpha \\ \theta \\ q \end{Bmatrix} + \begin{pmatrix} 0.052171 \\ 0 \\ 7.0084 \end{pmatrix} \mu_1. \tag{5.44}$$

3. Yaw dynamics:

$$\begin{Bmatrix} \dot{\psi} \\ \dot{\beta} \\ \dot{R} \end{Bmatrix} = \begin{pmatrix} 0 & 0 & 2.7285 \\ 0 & -0.0356 & -1 \\ 0 & -1.1961 & -0.0341 \end{pmatrix} \begin{Bmatrix} \psi \\ \beta \\ R \end{Bmatrix} + \begin{pmatrix} 0 \\ 0.052171 \\ -7.0084 \end{pmatrix} \mu_2. \tag{5.45}$$

Here, u_1 is the electrical signal input to the roll jet actuator, whose sign determines the direction of jet firing. The roll dynamics plant has a double pole at origin, $s_{1,2} = 0$, indicating an unstable open-loop plant. The eigenvalues of pitch and yaw dynamics are given by:

```
>> A=[-0.0356 -0.0233  1.0000; 0  0  1; 1.1961  0  -0.0341]; %Pitch dynamics
>> damp(A)

 Eigenvalue      Damping     Freq. (rad/s)
 -1.14e+000     1.00e+000      1.14e+000
  1.05e+000    -1.00e+000      1.05e+000
  2.34e-002    -1.00e+000      2.34e-002

>> Ay=[0  0  2.7285; 0  -0.0356  -1.0000;0  -1.1961  -0.0341]; %Yaw dynamics
>> damp(Ay)

 Eigenvalue      Damping     Freq. (rad/s)
  0.00e+000    -1.00e+000      0.00e+000
 -1.13e+000     1.00e+000      1.13e+000
  1.06e+000    -1.00e+000      1.06e+000
```

Hence, pitch and yaw plants are also unstable about the pitch equilibrium and have nearly identical eigenvalues.

5.4 Roll Control

The roll control system of a launch vehicle is quite similar to that of a reaction jet-controlled, single-axis spacecraft, although some aerodynamic damping in roll, $L_p < 0$, may be available due to stabilizing fins. Small roll perturbations can be caused by an asymmetric atmospheric gust acting on the aerodynamic fins, or by internal swirl moments generated by propellant consumption.

Example 5.2. For *Vanguard* rocket of Example 5.1, design a suitable roll control system for maintaining the vehicle in equilibrium roll attitude.

We see in Example 5.1 that the rocket is unstable in roll due to the absence of aerodynamic fins, thereby requiring active feedback stabilization. The roll controller is a switching system that maintains the vehicle within $\pm 3^\circ$ of roll error by applying a constant rolling moment via reaction jets. Such a control system is thus quite simple to implement and was discussed at length in Example 1.8.

Equation (5.43) is expressed as follows:

$$\ddot{\phi} = 0.1199 \operatorname{sgn}(u_1), \tag{5.46}$$

where $u_1(t)$ is the electrical signal input to the roll jet actuator determining the direction of control jets. Being nonlinear in nature, a switching control system can encounter the problem of *chatter*, i.e., rapid actuation even when a small error around the desired equilibrium state is detected, leading to a wastage of control effort. In order to avoid chatter, a dead-zone of $\pm 3^\circ$ is deliberately built in, resulting in the following control law:

$$u_1(t) = \begin{cases} > 0 & (\phi < -3^\circ) \\ 0 & (-3 \le \theta \le 3^\circ) \\ < 0 & (\theta > 3^\circ) \end{cases}$$

For simulating the closed-loop system, we refer the reader to Example 1.8. The closed-loop simulation results for 2 min of flight (assuming no change of roll parameters with time) are plotted in Figs. 5.4 and 5.5 for the initial perturbation of $\phi(0) = -2^\circ$ and $p(0) = 0.01$ rad/s. Note the subtle damping provided by the switching controller in the roll-rate response, which causes a delaying of successive jet pulses, thereby stabilizing the system about the zero roll state.

A linear feedback control law has an advantage over the switching controller in which it can achieve a more precise control with a smaller overall effort. However, it is much more difficult to implement a linear control law for a reaction jet system, because it requires a precise modulation of control torque magnitude by valves. Consider the following transfer function of the roll dynamics plant:

$$G(s) = \frac{\phi(s)}{\tau_x(s)} = \frac{\frac{1}{J_{xx}}}{s^2 - \frac{L_p}{J_{xx}} s}, \tag{5.47}$$

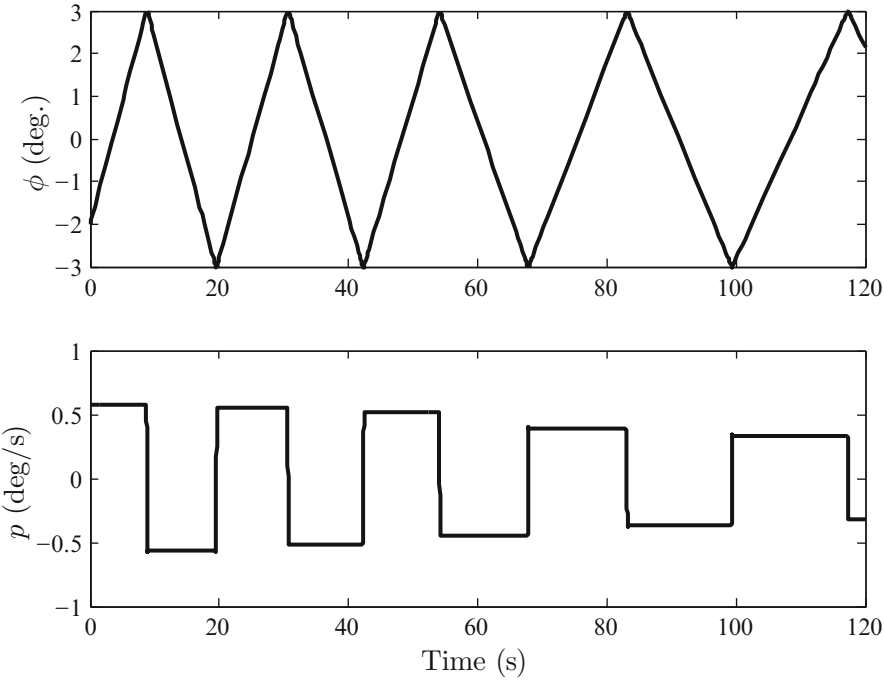

Fig. 5.4 Closed-loop initial response of the switching roll control system for *Vanguard* rocket

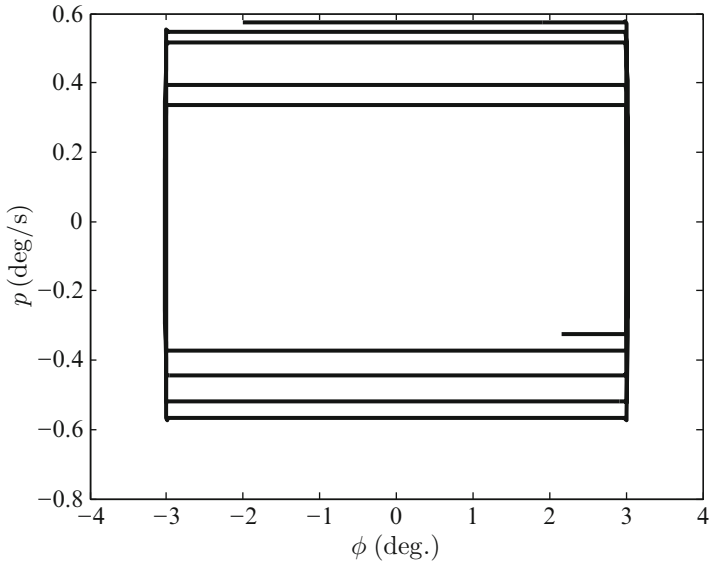

Fig. 5.5 Phase-plane plot, p vs. ϕ, of the switching roll control system for *Vanguard* rocket

where the yaw perturbation, ψ, is assumed zero. Since the plant possesses a pure integration in the open-loop, we can achieve a zero steady-state error to a step roll command, ϕ_d, by proportional feedback control,

$$\tau_x(s) = KE(s) = K[\phi_d s - \phi(s)], \tag{5.48}$$

which makes the closed-loop transfer function

$$\frac{\phi_{(s)}}{\phi_d(s)} = \frac{KG(s)}{1 + KG(s)} = \frac{\frac{K}{J_{xx}}}{s^2 - \frac{L_p}{J_{xx}}s + \frac{K}{J_{xx}}}, \tag{5.49}$$

asymptotically stable. As there can be large variations in the values of J_{xx} and L_p during flight, the feedback gain, K, must be carefully selected such that closed-loop performance does not deteriorate significantly at any point. The closed-loop characteristic equation,

$$s^2 - \frac{L_p}{J_{xx}}s + \frac{K}{J_{xx}} = s^2 + 2\zeta\omega s + \omega^2, \tag{5.50}$$

shows that while the settling-time,

$$t_s \simeq \frac{4}{\zeta\omega} = -\frac{8J_{xx}}{L_p}, \tag{5.51}$$

is unaffected by feedback gain, K, the value of the closed-loop damping ratio, ζ (thus the transient overshoots and control input magnitude), can be selected as desired through K as follows:

$$\zeta = -\frac{L_p}{2\sqrt{KJ_{xx}}}. \tag{5.52}$$

Of course, one can have a better closed-loop control using combined roll and roll rate feedback (i.e., a PD controller),

$$\tau_x(s) = (K_1 + sK_2)E(s), \tag{5.53}$$

with the closed-loop transfer function

$$\frac{\phi_{(s)}}{\phi_d(s)} = \frac{K_1 + sK_2}{J_{xx}s^2 + \left(K_2 - L_p\right)s + K_1}, \tag{5.54}$$

with a handle on both the settling-time,

$$t_s \simeq \frac{4}{\zeta\omega} = \frac{8J_{xx}}{K_2 - L_p}, \tag{5.55}$$

Table 5.1 Roll moment of inertia and damping in roll for Stage-I of a launch vehicle

$t(s)$	J_{xx} (kg m^2)	L_p (N m s/rad)
0	4937.6	−6.8801
6.0606	4856.5	−1469.8
12.121	4775.5	−2277.1
18.182	4694.4	−2338.5
24.242	4613.3	−1923.9
30.303	4532.3	−1358.5
36.364	4451.2	−854.08
42.424	4370.1	−489.62
48.485	4289.1	−260.37
54.545	4208	−130.15
60.606	4126.9	−61.817
66.667	4045.9	−28.148
72.727	3964.8	−12.381
78.788	3883.7	−5.2952
84.848	3802.7	−2.2145
90.909	3721.6	−0.9102
96.97	3640.5	−0.36923
103.03	3559.5	−0.14842

and the damping-ratio,

$$\zeta = \frac{K_2 - L_p}{2\sqrt{K_1 J_{xx}}}. \tag{5.56}$$

However, adding the roll rate feedback increases the input magnitude requirement, while introducing susceptibility (hence reduced robustness) to rate gyro noise. Using a suitable nonlinear switching strategy where a pendulum senses roll rate magnitude above a given threshold, one can improve closed-loop performance without requiring rate feedback. The design can be made more robust with respect to angular measurement noise by adding a suitable lag compensator as a pre-filter.

Example 5.3. Using the nominal data given in Table 5.1 for the first stage of a launch vehicle, design a roll control system to achieve a change in the roll angle by 1 rad before the first stage separation at $t = 103.03$ s. The vehicle is equipped with a roll control gas jet actuator with first-order time constant of 0.2 s, which can exert a maximum torque of ± 150 N m with a deadband of ± 5 N m (i.e., actuator does not respond to commanded torque less than 5 N m in magnitude). The closed-loop system must have adequate robustness with respect to roll angle measurement noise.

Before beginning the design, we analyze the plant's real pole, $s = L_p/J_{xx}$, plotted with time using spline interpolation in Fig. 5.6. Note the large variation in the pole's location during the first 60 s. If one takes an average value, −0.25, the following approximate plant settling-time can be expected

$$t_s \simeq -\frac{8}{0.25} = 32 \text{ s}.$$

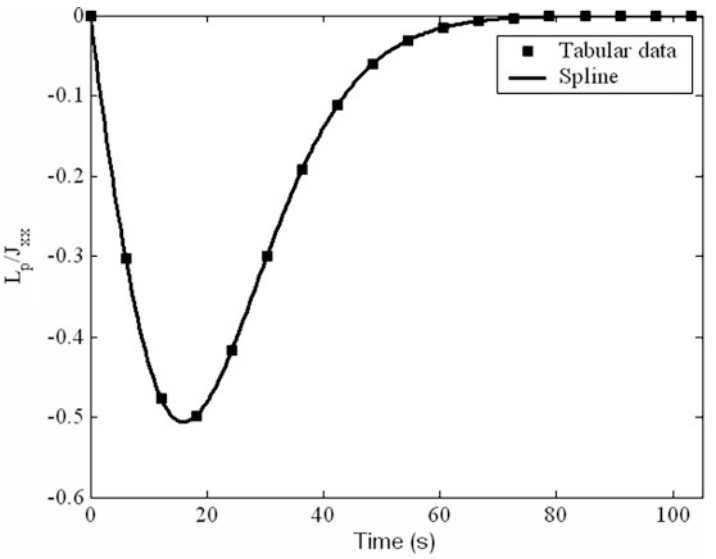

Fig. 5.6 Pole, $s = L_p/J_{xx}$, of roll dynamics plant for a gravity-turn launch vehicle

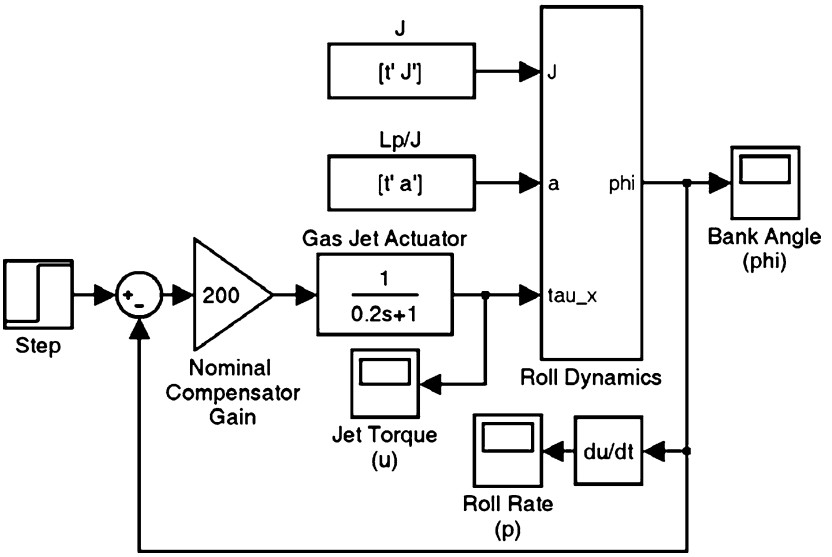

Fig. 5.7 Simulink block diagram of roll control system with proportional angle feedback for a launch vehicle

We will first examine proportional feedback with a constant gain, K, for which the Simulink block diagram is shown in Fig. 5.7. The roll dynamics plant used in the model is depicted in Fig. 5.8. The tabulated values of J_{xx} and $a = L_p/J_{xx}$ are

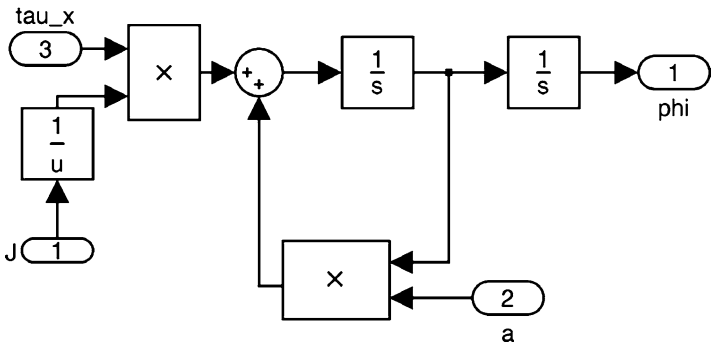

Fig. 5.8 Simulink block diagram of roll dynamics plant for a launch vehicle

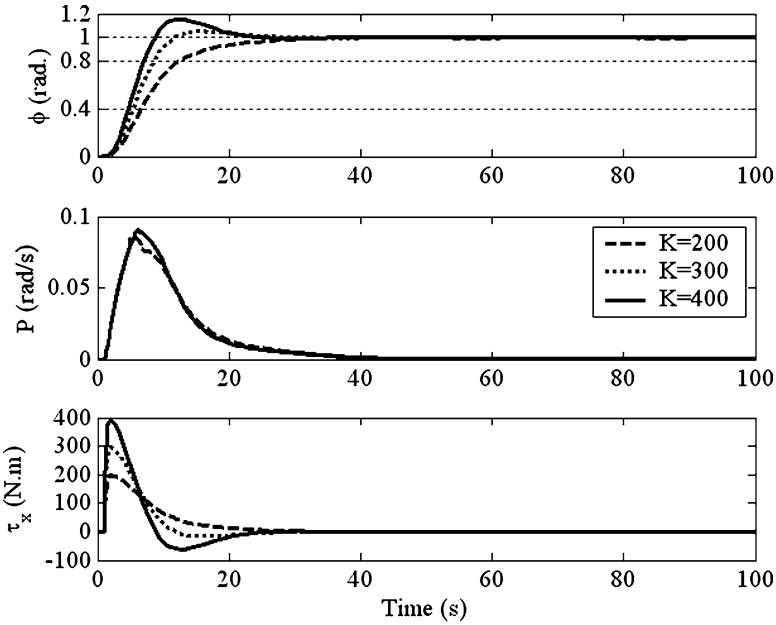

Fig. 5.9 Closed-loop response of roll control system with proportional feedback for a launch vehicle

stored in the MATLAB workspace as row vectors at the given time instants, t, and made available to the Simulink model as shown. Taking three different values of the gain, $K = 200, 300, 400$, the simulated closed-loop response without actuator nonlinearity and sensor noise is plotted in Fig. 5.9. Note that the maximum torque limit is exceeded in all cases, while $K = 200$ requires the minimum peak torque and also has the smallest overshoot, but an increased settling time. A further reduction in K tends to increase the error at $t = 100$ s, which is unacceptable. Therefore, we select $K = 200$ as our nominal design.

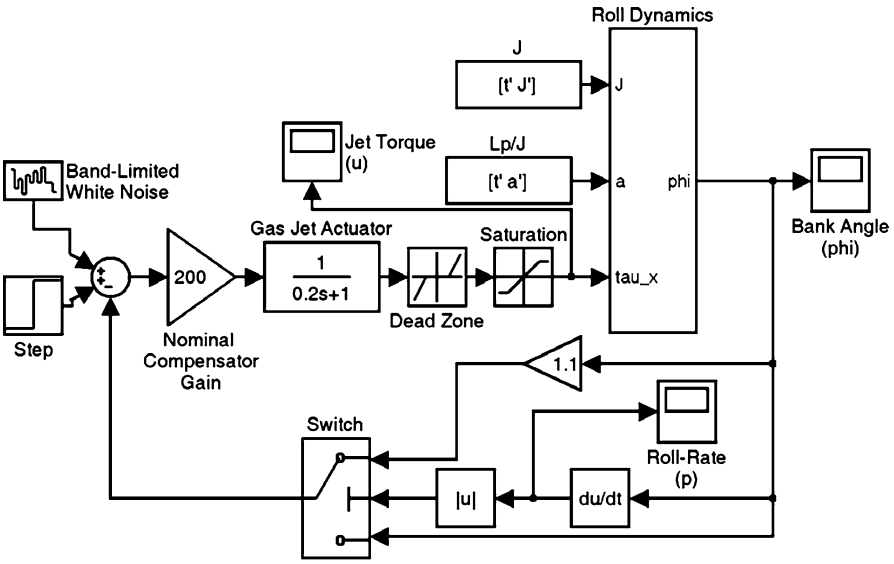

Fig. 5.10 Simulink block diagram of roll control system with proportional angle feedback and a roll rate-activated switch for a launch vehicle

An improvement over the nominal design is obtained by taking the roll rate magnitude into consideration. While not actually feeding back P, we use a pendulum-based switch (Fig. 5.10) that is activated when the roll rate magnitude exceeds 0.05 rad/s, in which case the feedback gain is increased by 10% for quickly reducing the transient error. Otherwise, the nominal gain ($K = 200$) is used. A comparison of the closed-loop response of the switched control system with actuator nonlinearities and that of the nominal linear design (without sensor noise) is plotted in Fig. 5.11. Note the slight increase in the settling time of the switched case with saturated control torque and deadband, as well as the reduction in the maximum pitch rate. Consequently, the transient angle response is much smoother than the nominal design.

Addition of sensor noise within the system's bandwidth can substantially degrade the closed-loop performance, especially in a time-varying plant controlled with a fixed feedback gain (as in the present case). In order to make the system robust with respect to noise in roll angle measurement, we add a lag compensator (Chap. 3) with the transfer function

$$H(s) = \frac{0.2s + 1}{s + 1}$$

as shown in the Simulink block diagram of Fig. 5.12. The lag compensator essentially moves the actuator pole from $s = -5$ to $s = -1$ with a unit DC gain, thereby decreasing control activity in response to the higher frequency noise input. In other words, the compensator decreases the control bandwidth by introducing phase lag and gain roll-off. The Bode plot of the lag compensator is given in Fig. 5.13 showing

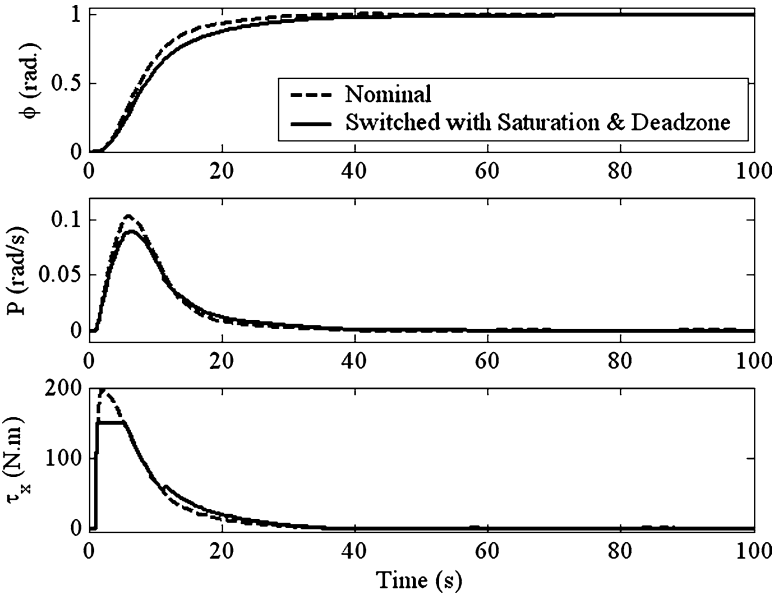

Fig. 5.11 Comparison of switched and unswitched roll control systems with proportional angle feedback for a launch vehicle

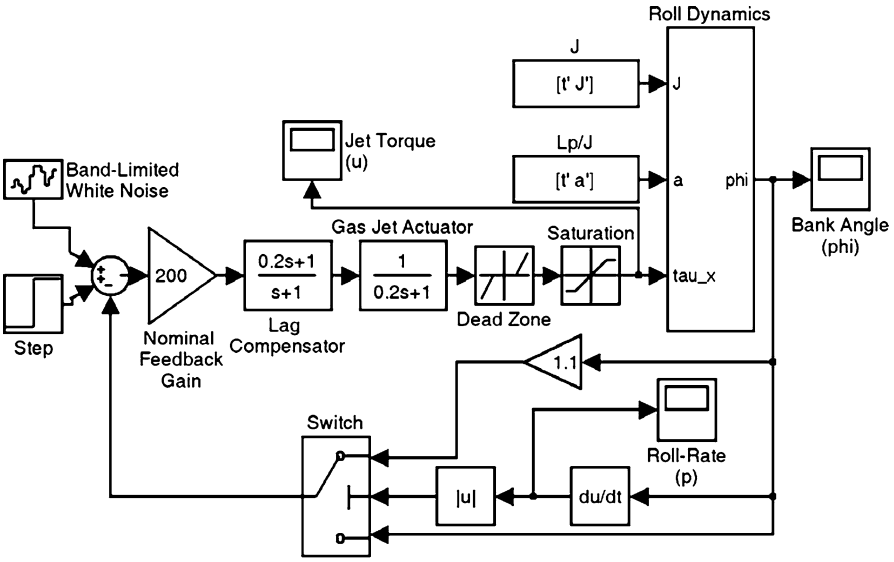

Fig. 5.12 Simulink block diagram of roll control system for a launch vehicle with proportional angle feedback, lag compensator, actuator nonlinearities, a roll rate-activated switch, and sensor noise

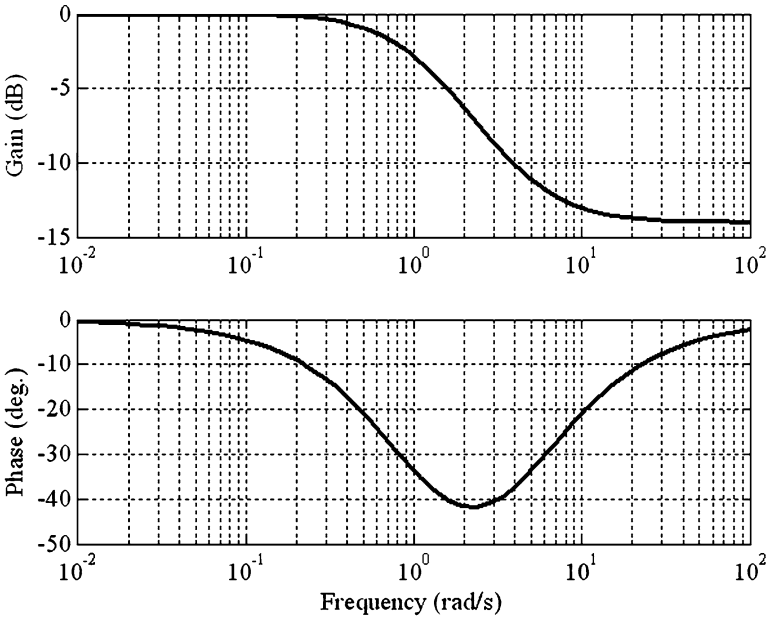

Fig. 5.13 Frequency response of the lag compensator for roll control system of a launch vehicle

a gain reduction by 14 dB in the frequency range $0.2 \leq \omega \leq 10$ rad/s and a phase dip of $-42°$ near $\omega = 2$ rad/s. The noise intensity for the simulation is specified by setting noise power spectral density as 10^{-4} rad in the *Band-Limited White Noise* block (Fig. 5.12), which corresponds to a rough angular resolution of 0.573°. A good IMU with optical angle encoder can produce a resolution about a fifth of this value. However, simulation for such a crude measurement would reveal the robustness (or lack thereof) of the closed-loop system. The noise sample interval is also conservatively selected to be 0.1 s, which is only half the actuator time constant. The response of the closed-loop system with (Fig. 5.12) and without (Fig. 5.10) the lag compensator is compared in Figs. 5.14 and 5.15. Note the significant improvement in the smoothness of the closed-loop torque input as well as a slight reduction in the peak roll rate caused by the lag compensator, albeit with an increase in settling time by 2–3 s.

5.5 Pitch-Yaw Control

A large rocket is designed to operate in a vertical plane in such a way that the normal acceleration required for maneuvering is naturally provided by the gravity component. This kind of trajectory is called a *gravity-turn*, and is used both for launching a payload to an orbit and for ballistic reentry missions. In order to fly a gravity-turn trajectory, the angle-of-attack and angle of sideslip must be kept zero,

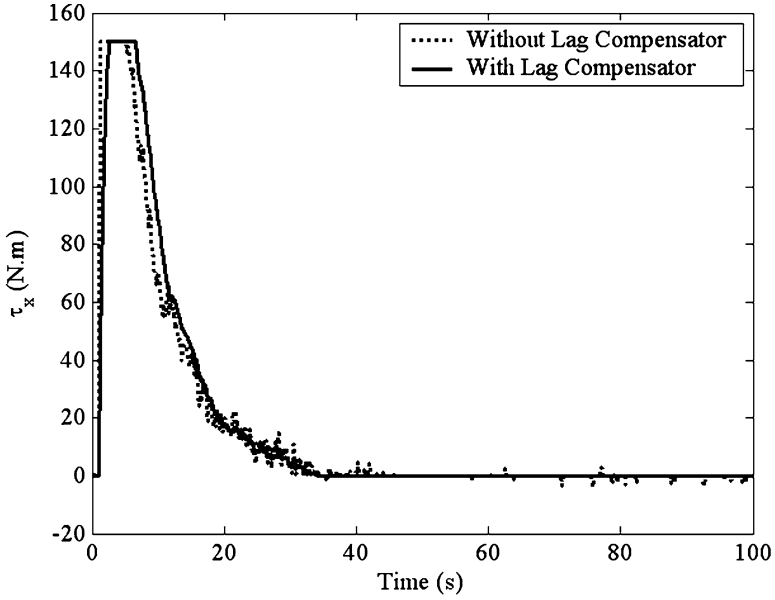

Fig. 5.14 Comparison of closed-loop rolling moment input of roll control systems with and without lag compensator

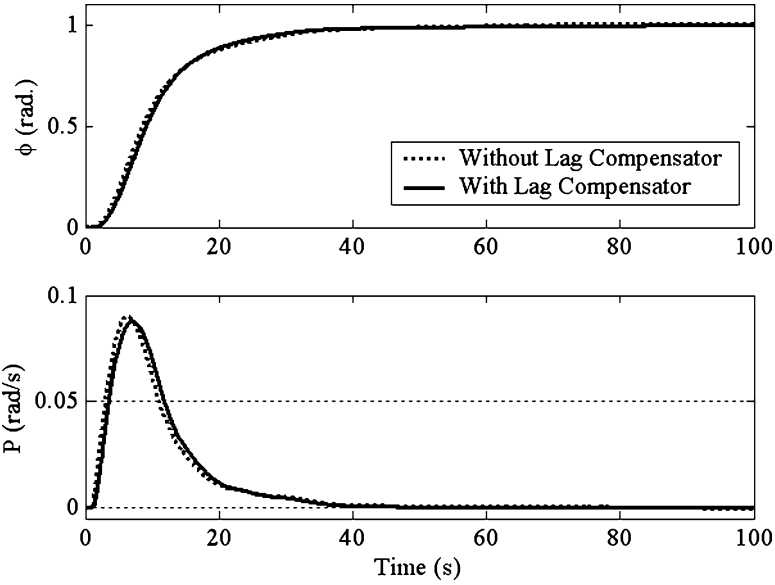

Fig. 5.15 Comparison of closed-loop roll angle and rate response of roll control systems with and without lag compensator

which requires matching the pitch angle, Θ, with the flight path angle (Chap. 2). The task of the control system is to align the longitudinal plane (or pitch plane) of the vehicle with the vertical plane of flight by nullifying roll and yaw motions, while generating the required pitch rate through gimbaling. The nominal trajectory for a given mission is either pre-computed and stored onboard, or supplied to the vehicle via a radio link from the ground station. We will study the design of the pitch control system, and note that yaw control is quite similar (if not identical) to the pitch regulator.

We have the following equations of zero-lift translation (Chap. 2) in a vertical plane with radius,[3] $r(t)$, latitude, $\delta(t)$, airspeed, $v(t)$, and flight path angle, $\gamma(t)$, relative to a planet-fixed frame with origin at the center of the spherical planet:

$$\begin{aligned}
\dot{r} &= v \sin\gamma \\
\dot{\delta} &= \frac{v}{r}\cos\gamma \\
\frac{(T-D)}{m} - g\sin\gamma &= \dot{v} + \Omega^2 r\cos\delta(\cos\gamma\cos\psi\sin\delta - \sin\gamma\cos\delta) \\
g\cos\gamma &= -v\dot{\gamma} + \frac{v^2}{r}\cos\gamma + 2\Omega v\sin\gamma\cos\delta \\
&\quad + \Omega^2 r\cos\delta(\sin\gamma\cos\psi\sin\delta + \cos\gamma\cos\delta), \qquad (5.57)
\end{aligned}$$

where ψ is the constant flight direction, T the thrust, and D the atmospheric drag. The equations include the Coriolis and centripetal acceleration due to planetary rotation, Ω. The nominal trajectory,

$$[r_d(t), \delta_d(t), v_d(t), \gamma_d(t)],$$

is an optimal solution of these equations for specific boundary conditions.

Consider the stability axis, $(\mathbf{i_d}, \mathbf{j_d}, \mathbf{k_d})$, with $\mathbf{i_d}$ always along the nominal flight direction and $\mathbf{j_d}$ normal to the plane of flight. The axis, $\mathbf{k_d}$, completes the right-handed triad, $\mathbf{k_d} = \mathbf{i_d} \times \mathbf{j_d}$. Such a frame describes the nominal attitude of the vehicle required for tracking the nominal trajectory. With a nominal pitch rate, $Q_d(t)$, the angular velocity of the stability axes is given by

$$\boldsymbol{\omega}_{\mathrm{d}} = Q_d \mathbf{j_n}. \qquad (5.58)$$

The nominal pitch rate is continuously updated by the guidance system such that it always equals the rate of change of flight path angle (5.57):

$$\begin{aligned}
Q_d = \dot{\gamma}_d &= \left(\frac{v_d}{r_d} - \frac{g_0 r_0^2}{v_d r_d^2}\right)\cos\gamma_d + 2\Omega v_d \sin\gamma_d \cos\delta_d \\
&\quad + \Omega^2 r_d \cos\delta_d(\sin\gamma_d\cos\psi_d\sin\delta_d + \cos\gamma_d\cos\delta_d). \qquad (5.59)
\end{aligned}$$

[3] In order to avoid confusion, we have denoted yaw-rate perturbation as $R(t)$.

Tracking a reference pitch rate command is called a *pitch program* and is used in one way or the other by all launch vehicles. By integrating the pitch rate signal, the desired pitch angle, Θ_d, can also be obtained at each time instant. However, instead of maintaining a pitch equilibrium, the pitch program is intended for varying the pitch rate in a specific fashion, which requires generating a nominal pitching moment through gimbaling. The nominal gimbal profile can be calculated by putting $\alpha = 0$ and $\dot{\alpha} = 0$ in the pitching moment equation:

$$\mu_{1_d} = \frac{J_{yy}\dot{Q}_d - M_q Q_d}{T\xi}. \tag{5.60}$$

By neglecting the instantaneous variation of $Q_d(t)$ due to planetary rotation, radius, and airspeed, we write

$$\dot{Q}_d \simeq \frac{\partial Q_d}{\partial \gamma_d}\dot{\gamma}_d = -Q_d\left(\frac{v_d}{r_d} - \frac{g_0 r_0^2}{v_d r_d^2}\right)\sin\gamma_d = -Q_d^2\tan\gamma_d, \tag{5.61}$$

we have the following gimbaling command for the pitch program:

$$\mu_{1_d} = -\frac{(J_{yy}Q_d\tan\gamma_d + M_q)Q_d}{T\xi}. \tag{5.62}$$

This is quite easy to implement in a guidance computer, where $Q_d(t)$ profile can be stored and the current flight path angle fed back by a rate-integrating gyro. A similar pitch program was implemented in the earliest guided rocket vehicles (such as the German *V-2* rocket) by a clockwork mechanism driving the pitch gimbal via rate-integrating gyro signal. With the availability of digital computers, it is now routine to perform online computations of the desired pitch attitude.

We can now contemplate the guidance and control system for pitch-yaw dynamics, shown as a schematic block diagram in Fig. 5.16. The feedforward part of the system is the pitch program consisting of (5.59) and (5.60), which are supplied by the guidance computer. Additionally, the guidance system can issue gimbal commands, $\mu_{1d}(t), \mu_{2d}(t)$, to correct small deviations from the nominal trajectory. The task of the pitch-yaw controller is to drive the angular rate error, q, R, to zero as quickly as possible by corrective gimbaling. Such a controller uses pitch and yaw angles or rates, as well as normal acceleration, $\mathbf{a_n}(t)$, for feedback. The outer guidance loop senses flight path errors, $\gamma(t), \psi(t)$, via rate-integrating gyros to correct flight path deviations.

Example 5.4. Consider the pitch control of the first stage of *Vanguard* rocket (Example 5.1) for flying a gravity-turn trajectory specified in Table 5.2. The duration of flight is small enough for the planetary rotation effects to be negligible. Thus, we have

$$Q_d = \dot{\gamma}_d = \left(\frac{v_d}{r_d} - \frac{g_0 r_0^2}{v_d r_d^2}\right)\cos\gamma_d, \tag{5.63}$$

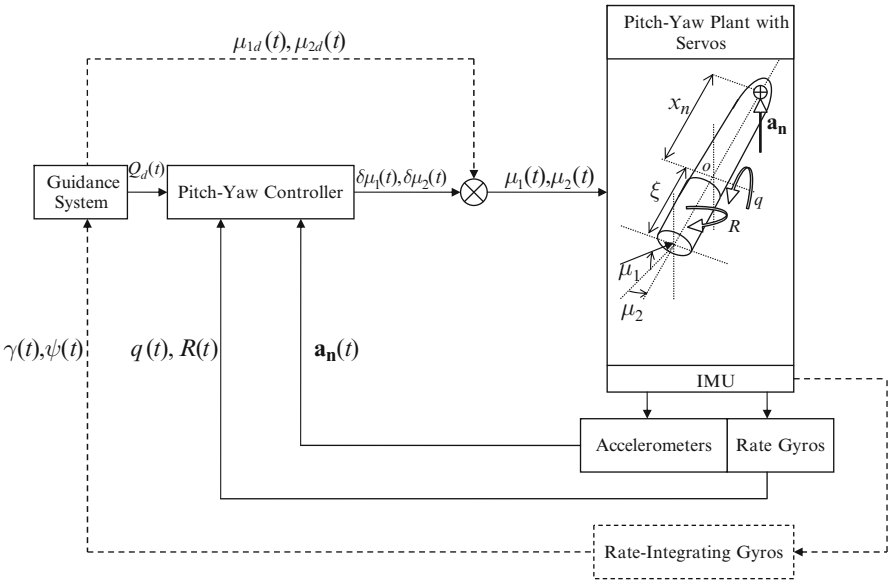

Fig. 5.16 A typical pitch-yaw guidance and control system for a gravity-turn launch vehicle

Table 5.2 Nominal gravity-turn trajectory for Stage I flight of the *Vanguard* rocket

$t\,(s)$	r (km)	v (km/s)	γ (rad)
11.347	6378.6	0.088604	1.5349
14.047	6378.9	0.10625	1.5237
16.747	6379.2	0.12437	1.5115
19.447	6379.5	0.14287	1.4985
22.147	6379.9	0.16166	1.4848
24.847	6380.4	0.18074	1.4704
27.547	6380.9	0.20012	1.4555
30.247	6381.5	0.21983	1.4401
32.947	6382.1	0.24004	1.4242
35.647	6382.8	0.2608	1.408
38.347	6383.5	0.28225	1.3915
41.047	6384.3	0.30443	1.3747
43.747	6385.1	0.32742	1.3577
46.447	6386	0.35114	1.3407
49.147	6386.9	0.37494	1.3235
51.847	6388	0.39865	1.3063
54.547	6389	0.42268	1.289
57.247	6390.1	0.44717	1.2717
59.947	6391.3	0.47264	1.2544
62.647	6392.6	0.49934	1.2372
65.347	6393.9	0.52757	1.22

(continued)

Table 5.2 (continued)

$t(s)$	r (km)	v (km/s)	γ (rad)
68.047	6395.2	0.55753	1.2031
70.747	6396.7	0.58946	1.1863
73.447	6398.2	0.62356	1.1698
76.147	6399.8	0.65985	1.1536
78.847	6401.5	0.6983	1.1378
81.547	6403.2	0.73892	1.1223
84.247	6405.1	0.7817	1.1072
86.947	6407	0.82663	1.0926
89.647	6409	0.87368	1.0784
92.347	6411.1	0.92285	1.0646
95.047	6413.4	0.97414	1.0512
97.747	6415.7	1.0276	1.0383
100.45	6418.2	1.0832	1.0258
103.15	6420.7	1.1411	1.0138
105.85	6423.4	1.2014	1.0021
108.55	6426.2	1.2641	0.99093
111.25	6429.1	1.3295	0.98013
113.95	6432.1	1.3975	0.96973
116.65	6435.3	1.4685	0.95973
119.35	6438.6	1.5425	0.95013
122.05	6442.1	1.6196	0.94091
124.75	6445.7	1.7002	0.93206
127.45	6449.5	1.7843	0.92359
130.15	6453.4	1.8722	0.91548
132.85	6457.5	1.964	0.90772
135.55	6461.8	2.0601	0.90031
138.25	6466.2	2.1607	0.89324
140.95	6470.9	2.2662	0.8865
143.65	6475.7	2.377	0.88009
146.35	6480.8	2.4937	0.874

where $r_0 = 6378.14$ km and $g_0 = 9.806$ m/s^2. The thrust is maintained constant at $T = 133202.86$ N, while the variations of the mass and the pitch moment of inertia are the following:

$$m = 7727.3[1 - 0.0054(t - 11.347)] \text{ kg}$$
$$J_{yy} = 215000[1 - 0.006(t - 11.347)] \text{ kg m}^2.$$

The 1976 US standard atmosphere model [21] is used to generate the dynamic pressure, $\bar{q}$, and Mach number, $\mathcal{M}$, along the nominal trajectory for the first 200 s of flight, which are plotted in Fig. 5.17. The variations of the drag, D, and the stability derivatives, Z_α, M_α, M_q, along the nominal trajectory are plotted in Fig. 5.18. Note the sharp transonic drag rise as well as the large changes in the stability derivatives near $\mathcal{M} = 1$ ($t = 50$ s). Also note the maximum dynamic pressure flight

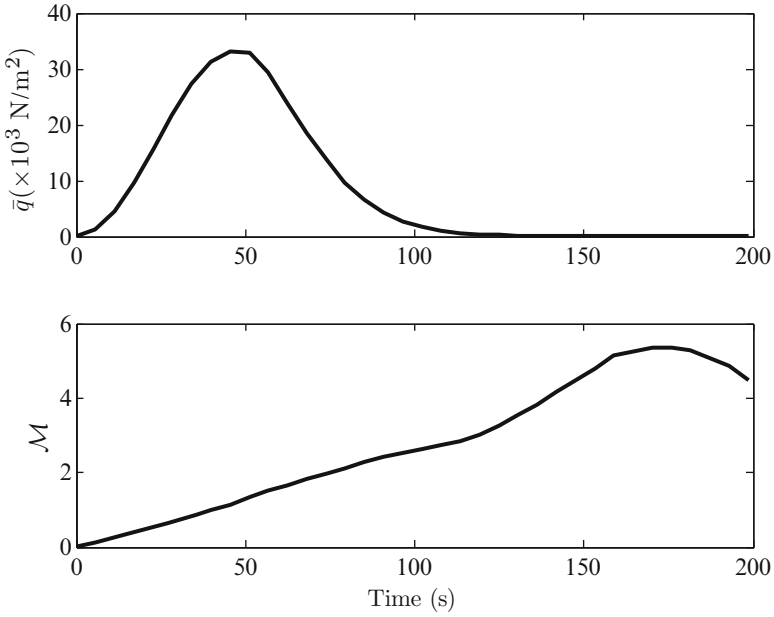

Fig. 5.17 The dynamic pressure and Mach number profiles for the nominal flight of the *Vanguard* rocket

point near $t = 50$ s. The portion of flight lying between the transonic and the maximum dynamic pressure corresponds to the region of the largest aerodynamic loads experienced by the vehicle. There is another smaller drag peak at the onset of hypersonic regime ($t = 125$ s) corresponding to the point of maximum aerodynamic heating.

A Simulink block diagram coded for simulating the ballistic, gravity-turn flight path in the vertical plane is depicted in Fig. 5.19. Note the absence of planetary rotation (thus the latitude) in this basic trajectory model. Here, "u1" and "u2" denote the nominal axial and normal acceleration inputs applied by the rocket thrust and the atmosphere, while "rout," "vout," and "gamout" are the radius, airspeed, and flight path angle, respectively. The initial conditions are specified in the respective integrator blocks at $t = 11.347$ s as per Table 5.2.

With $M_{\dot{\alpha}} \simeq 0$, the pitch dynamics plant about the nominal trajectory is given by

$$\begin{Bmatrix} \dot{\alpha} \\ \dot{\theta} \\ \dot{q} \end{Bmatrix} = \begin{pmatrix} \dfrac{Z_\alpha}{mv_d} & -\dfrac{g}{v_d}\sin\Theta_d & 1 \\ 0 & 0 & 1 \\ \dfrac{M_\alpha}{J_{yy}} & 0 & \dfrac{M_q}{J_{yy}} \end{pmatrix} \begin{Bmatrix} \alpha \\ \theta \\ q \end{Bmatrix} + \begin{pmatrix} \dfrac{T}{mv_d} \\ 0 \\ \dfrac{T\xi}{J_{yy}} \end{pmatrix} \delta\mu_1, \tag{5.64}$$

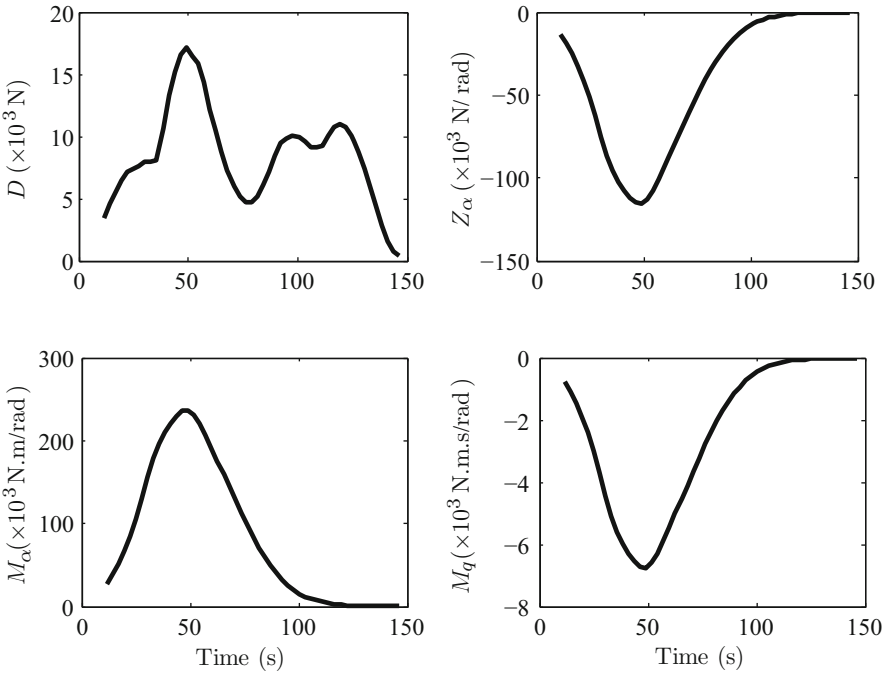

Fig. 5.18 The atmospheric drag and stability derivatives along the nominal trajectory of the *Vanguard* rocket

where $\delta\mu_1$ is the corrective gimbal input for attitude control. The vehicle is equipped with first-order pitch and yaw gimbal servos, each of time constant 0.02 s. Let us design a pitch controller for the rocket such that the angle-of-attack and pitch deviations are brought to within $\pm 1°$ with the gimbal angle not exceeding $\pm 5°$.

We select pitch angle error as the sole output, $y(t) = \theta(t)$, which is measured via a rate-integrating gyro. A regulator and a full-order observer are then designed using the plant dynamics in the maximum dynamic pressure region, $t \simeq 50$ s, by the frozen LQR method (Chap. 3). The plant parameters at the selected design point have already been derived in Example 5.1. The initial response of the closed-loop system (with servo) to a 5.7° initial angle-of-attack perturbation is plotted in Fig. 5.20. The closed-loop frequency response at the design point is plotted in Fig. 5.21, showing a gain margin of 37.9 dB and a phase margin of 175°. While the gain margin may be adequate for the model parameter variation (process noise) envisaged here, it can be improved by adding a pitch-rate feedback loop. A Simulink model (Fig. 5.22) is created for the pitch dynamics plant such that its coefficients, $m, U, J_{yy}, Z_\alpha, M_\alpha$, and M_q, are continuously updated along the nominal trajectory according to Table 5.2, (5.64) and Fig. 5.18. Finally, the pitch control system is simulated along with gimbal saturation limits using the Simulink block diagram of

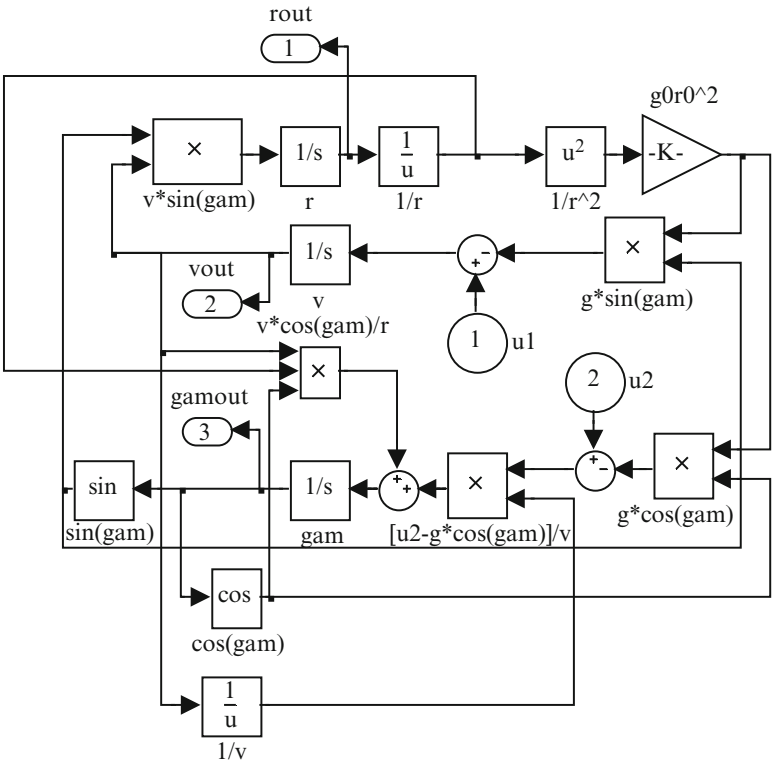

Fig. 5.19 Simulink block diagram for simulating the nominal trajectory of the *Vanguard* rocket

Fig. 5.23, and the results are plotted in Figs. 5.24 and 5.25. The design steps are given by the following MATLAB-CST statements:

```
>> A =[-0.0356   -0.0233    1.0000
                0          0    1.0000
           1.1961          0   -0.0341];

>> B=[0.0522   0    7.0084]';
>> C=[0  1  0]; D=0;
>> [k,S,E]=lqr(A,B,[0.01 0 0;0 0.1 0;0 0 0.1],1) %Regulator design by LQR

k =
    0.1954    0.3456    0.4993

S =
    0.4326   -0.4183    0.0247
   -0.4183    0.5933    0.0524
    0.0247    0.0524    0.0711

E =
   -2.4910
   -0.0397
   -1.0488
```

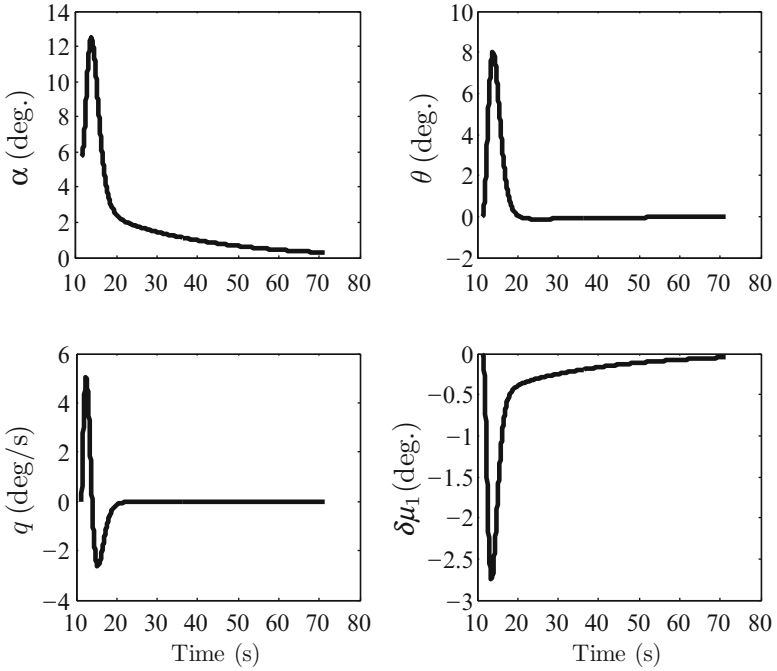

Fig. 5.20 Closed-loop initial response (with servo) of the pitch control system at the design point for Stage I of the *Vanguard* rocket

```
>> Lp=lqr(A',C',eye(3),1);L=Lp' %Observer (Kalman Filter) design by LQR

L =
    4.5545
    3.3159
    4.9975

% Augmented plant with gimbal servo follows:
>> Abar=[A B;zeros(1,3) -50]

Abar =
   -0.0356   -0.0233    1.0000    0.0522
         0         0    1.0000         0
    1.1961         0   -0.0341    7.0084
         0         0         0  -50.0000

>> Bbar=[0 0 0 50]'

Bbar =
     0
     0
     0
    50

>> Cbar=[C 0]

Cbar =
     0     1     0     0
```

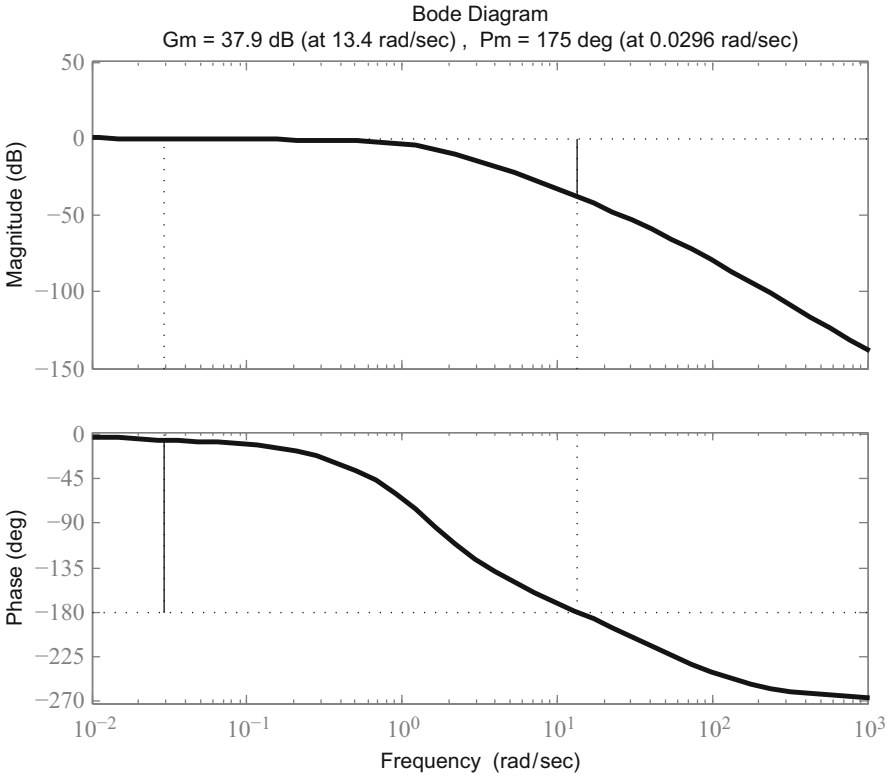

Fig. 5.21 Closed-loop frequency response and gain and phase margins of the pitch control system at the design point for Stage I of the *Vanguard* rocket

```
>> Ac=[Abar  -Bbar*k;L*Cbar A-L*C-B*k] %Servo augmented closed-loop system

Ac =
   -0.0356   -0.0233    1.0000    0.0522         0         0         0
         0         0    1.0000         0         0         0         0
    1.1961         0   -0.0341    7.0084         0         0         0
         0         0         0  -50.0000   -9.7704  -17.2824  -24.9673
         0    4.5545         0         0   -0.0458   -4.5958    0.9739
         0    3.3159         0         0         0   -3.3159    1.0000
         0    4.9975         0         0   -0.1734   -7.4199   -3.5337

>> Bc=[Bbar*k; B*k]
Bc =
         0         0         0
         0         0         0
         0         0         0
    9.7704   17.2824   24.9673
    0.0102    0.0180    0.0261
         0         0         0
    1.3695    2.4224    3.4996

>> sys=ss(Ac,Bc(:,2),[0 1 0 zeros(1,4)],0) %Closed-loop system with pitch
   angle output
```

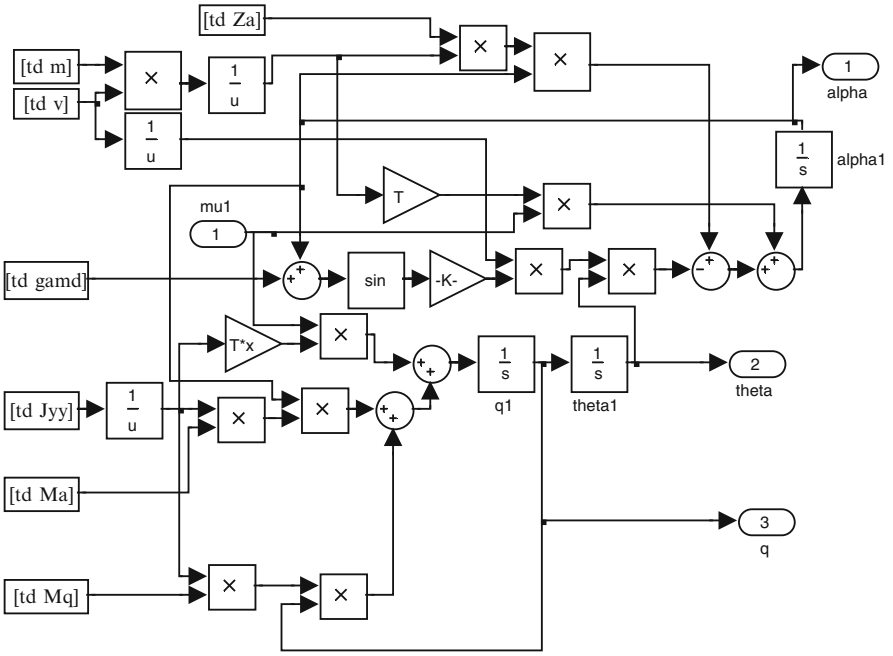

Fig. 5.22 Simulink block diagram for simulating the pitch dynamics plant for Stage I of the *Vanguard* rocket along the nominal trajectory

```
a =
           x1        x2        x3        x4        x5        x6        x7
   x1 -0.03561  -0.02327         1   0.05217         0         0         0
   x2         0         0         1         0         0         0         0
   x3     1.196         0  -0.03407     7.008         0         0         0
   x4         0         0         0       -50     -9.77    -17.28    -24.97
   x5         0     4.554         0         0   -0.0458    -4.596    0.9739
   x6         0     3.316         0         0         0    -3.316         1
   x7         0     4.997         0         0   -0.1734     -7.42    -3.534

b =
           u1
   x1       0
   x2       0
   x3       0
   x4   17.28
   x5  0.01803
   x6       0
   x7   2.422

c =
       x1  x2  x3  x4  x5  x6  x7
   y1   0   1   0   0   0   0   0

d =
       u1
   y1   0

Continuous-time model.
>> [y,t,x]=initial(sys,[0.1 0 0 0 0 0 0]'); %Closed-loop initial response
>> margin(sys) % Closed-loop freq. response with gain and phase margins
```

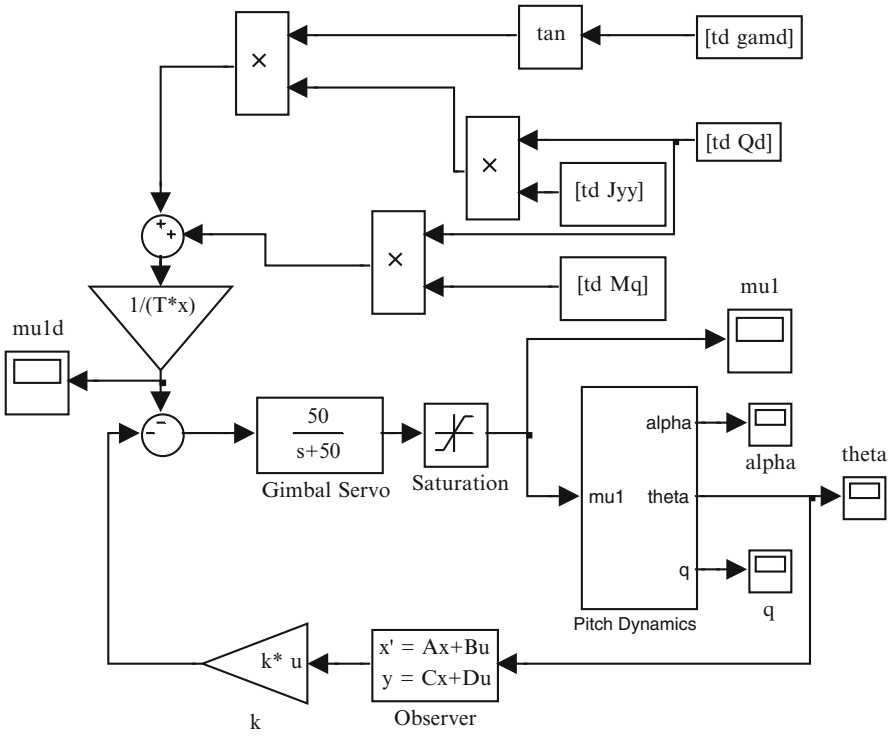

Fig. 5.23 Simulink block diagram for simulating the closed-loop pitch control system for Stage I of the *Vanguard* rocket

The nominal flight path angle, pitch-rate, and nominal gimbal angle are shown in Fig. 5.24. Figure 5.25 shows that the pitch controller – based on fixed regulator and observer gains – is able to quickly reduce the angle-of-attack and pitch-rate errors, and maintains them at nearly zero level throughout the flight, despite a large variation in the inertial and aerodynamic parameters. Only toward the end of the I stage flight, a slight oscillation is evident in the pitch angle due to a significantly reduced aerodynamic damping (M_q). The gimbal angle response never reaches the saturation level for the rather large initial angle-of-attack perturbation (5.7°). Thus, our design is quite successful. However, the pitch controller needs to be simulated in the guidance loop for a better assessment of its performance.

5.6 Summary

Flight of most rockets is largely confined to the vertical (longitudinal) plane and is usually ballistic in nature (zero lift and side force) to avoid excessive transverse loads. The guidance and control system must maintain the vehicle on a ballistic

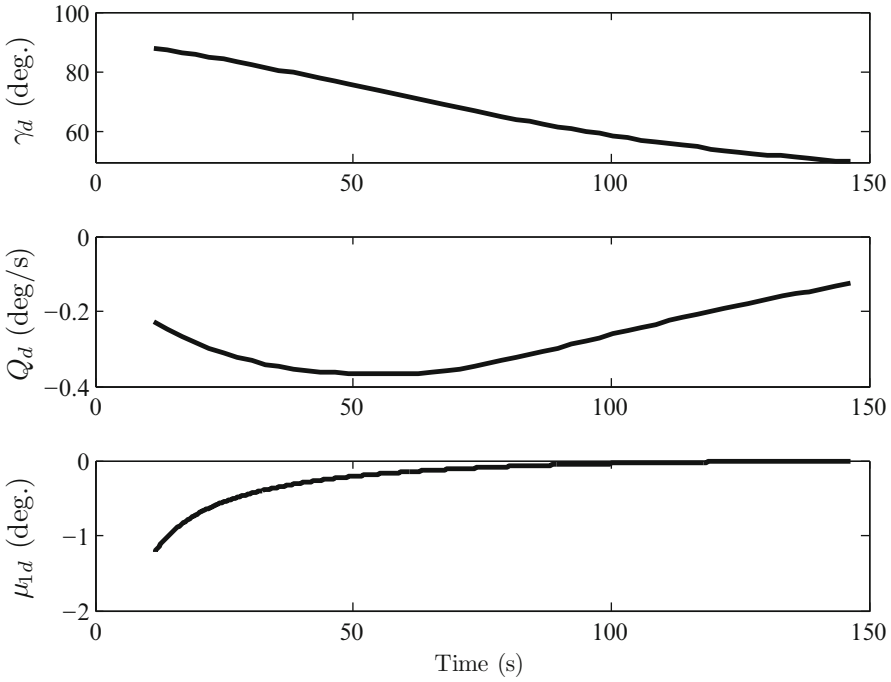

Fig. 5.24 Nominal gravity-turn flight path angle, desired pitch-rate, and gimbal angle along the nominal trajectory of Stage I of the *Vanguard* rocket

trajectory – called the gravity turn – that allows the flight path angle to change naturally from a near vertical to horizontal in a given time, under the sole influence of gravity. Due to the decoupling of roll dynamics from pitch and yaw, as well as pitch and yaw symmetry, it is possible to have separate control loops for roll, pitch, and yaw, and nearly identical regulators for pitch and yaw. While roll control is performed by either switching or linear feedback, pitch and yaw control is primarily based on driving the gimbal actuators via a linear feedback control law based on sensed attitude errors. A typical rocket is a time-varying plant due to the varying inertial and aerodynamic parameters. However, since the duration of each stage is of only a few minutes, a controller based upon fixed regulator and observer gains at the highest dynamic pressure design point is sufficient for attitude control.

Exercises

5.1. Consider a rocket with four gimbaled engines of identical, constant thrust, $T/4$, mounted symmetrically at the circular base in a ring with distance d from the base center, and a distance ξ from the center of mass. The thrust direction

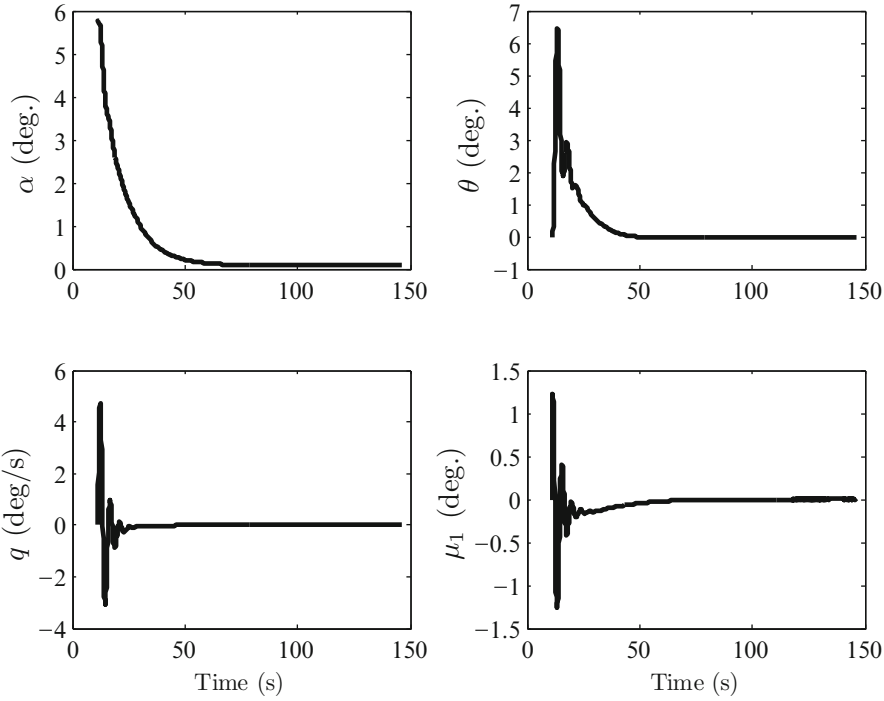

Fig. 5.25 Simulated closed-loop initial response (with servo saturation) of the frozen LQR pitch control system along the nominal trajectory of Stage I of the *Vanguard* rocket

of ith engine is controlled by swivel angle, δ_{i}, and deflection angle, μ_i, such that

$$\mathbf{T_i} \simeq \frac{T}{4}\left(\mathbf{i} - \mu_i \cos\delta_{\mathrm{i}}\mathbf{j} - \mu_i \sin\delta_{\mathrm{i}}\mathbf{k}\right).$$

Selecting the body axis oz along the direction from engine number 1 to engine number 3, and oy from 4 to 2, show that the net torque is given by

$$\begin{aligned}\boldsymbol{\tau} \simeq\ & \frac{T}{4}\xi \sum_{i=1}^{4} \mu_i \left(\cos\delta_{\mathrm{i}}\mathbf{k} - \sin\delta_{\mathrm{i}}\mathbf{j}\right) \\ & + \frac{T}{4} d \left(\mu_4 \sin\delta_4 + \mu_3 \cos\delta_3 - \mu_1 \cos\delta_1 - \mu_2 \sin\delta_2\right)\mathbf{i}.\end{aligned}$$

What is the net torque when gimbaling is carried out for transverse force balance?

5.2. Can a gimbal system be designed to maneuver a rocket sideways, but without rotating it on its axis? (This would be the case of a net transverse force with a zero moment.)

5.3. Consider a roll dynamics plant with $J_{xx} = 300$ kg m^2 and $L_p = -400$ N m s/rad. Design a suitable roll controller for achieving a desired step change of roll angle by 10° in about 1 s, without exceeding the maximum control rolling moment, $|\tau_x| \leq 4$ N m.

5.4. Consider a simplified pitch dynamics plant with $\alpha \approx 0$ and the following transfer function:

$$\frac{\theta(s)}{\mu_{1d}(s)} = -\frac{T\xi/J_{yy}}{s^2 - \frac{M_q}{J_{yy}}s}.$$

where $T = 2{,}000$ N, $J_{yy} = 6{,}000$ kg m^2, $\xi = 1$ m, and $M_q = -2{,}000$ N m s/rad. Design a suitable pitch controller for achieving a desired step change of pitch angle by 10° in about 1 s, without the pitch gimbal angle exceeding ±1°.

5.5. Why do rockets need a guide-rail (or launcher) when being launched vertically, and not when launched at an angle? Try to answer this in the light of translational dynamics in a vertical plane (do not include planetary rotation effects).

5.6. Modify the Simulink block diagram given in Fig. 5.19 to simulate the gravity-turn trajectory of a rocket from Earth's surface with a constant thrust of 10,000 N, a linearly varying mass from launch $t = 0$ until burnout, $t = 300$ s, given by

$$m(t) = 1{,}000 - 2.5t \text{ (kg)}; \qquad (0 \leq t \leq 300 \text{ s}),$$

and the following approximate aerodynamic drag given by the exponential atmospheric model:

$$D(t) = 0.25\mathrm{e}^{-h/6700}v^2 \text{ (N)}; \qquad (0 \leq t \leq 300 \text{ s}),$$

where h is the altitude in m and v is the airspeed in m/s. Assume initial conditions of $h(0) = 0, v(0) = 10$ m/s and $\gamma(0) = 85°$ (which must be specified in the respective integrator blocks). The normal acceleration input should be set as "u2 = [0 0]" in the MATLAB workspace, while the axial acceleration input, "u1," must be programmed using the relevant mathematical function blocks from the Simulink library. Plot the trajectory variables, $h(t), v(t), \gamma(t)$. What are the final airspeed and flight path angle?

5.7. Redesign the pitch controller for the Vanguard rocket of Example 5.4 by pole placement. Select optimal regulator and observer poles for meeting the design requirements. Compare the closed-loop design with that of Example 5.4.

5.8. Replace the pitch controller design for the Vanguard rocket of Example 5.4 using pitch-rate instead of pitch angle as the output variable. Select suitable cost matrices for LQR design of regulator and observer for meeting the design requirements. What are the gain and phase margins of the closed-loop system? Simulate and compare the closed-loop system with that of Example 5.4.

5.9. Redesign the pitch controller of Example 5.4 by adding the pitch-rate (along with the pitch angle) as an output variable. For the resulting two-output, single-input plant, select suitable cost matrices for LQR design of regulator and observer for meeting the design requirements. Simulate the closed-loop system along the nominal trajectory. Is there any improvement in the performance (transient response) and robustness (gain and phase margins at design point) compared to the designs of Example 5.4 and Exercise 5.8?

5.10. Replace the pitch controller design for the Vanguard rocket of Example 5.4 using a normal acceleration output, $a_z = U(\dot{\alpha} - x_n \dot{q})$, from a sensor located a distance, x_n, forward of the center of mass. Select suitable cost matrices for LQR design of regulator and observer for meeting the design requirements. What are the gain and phase margins of the closed-loop system? Simulate and compare the closed-loop system with that of Example 5.4.

5.11. Design a yaw controller for the Vanguard rocket of Example 5.4 using the frozen LQR method (Chap. 3) using the yaw rate as the feedback signal from IMU. Select the cost coefficient matrices such that the maximum gimbal angle of $\pm 5^\circ$ is never exceeded for an initial sideslip angle of 5.7°. Compare your design with that given in Example 5.4 for pitch control. Simulate the closed-loop response with the given yaw gimbal servo.

5.12. Redesign the yaw controller of Exercise 5.11 using the lateral normal acceleration output, $a_y = U(\dot{\beta} + x_n \dot{R})$, from a sensor located a distance, x_n, forward of the center of mass. Compare your design with that of Exercise 5.11 and simulate the closed-loop response along the nominal trajectory.